Transactions of the Royal Society of Edinburgh: Earth Sciences, **95**, 393–421, 2005 (for 2004)

Palaeoproterozoic, rift-related, ^{13}C-rich, lacustrine carbonates, NW Russia. Part I: Sedimentology and major element geochemistry

V. A. Melezhik and A. E. Fallick

ABSTRACT: The 150-m-thick Kuetsjärvi Sedimentary Formation (KSF) from the Pechenga Greenstone Belt, NW Russia, is one of the key formations in the study of a positive $\delta^{13}C_{carb}$ excursion occurring globally in the Palaeoproterozoic. The KSF formed in an intracratonic rift setting and is sandwiched between two, 2-km-thick subaerially erupted volcanic units. The KSF was previously interpreted as shallow marine, but new data reported here indicate that it is a non-marine unit deposited on a deeply subaerially weathered surface mantling the underlying volcanic rocks. The lowermost part of the KSF represents an alluvial–fluvial plain, followed by a laterally and vertically variable succession of variegated to mottled fine-grained siliciclastic rocks and 'red beds', dolostones containing stromatolite sheets, hydrothermal travertine deposits and abundant desiccation features (e.g. tepees, surfical silicified crusts and dissolution cavities), including probable pseudomorphed evaporites. Measured S and C_{org} concentrations for the carbonate and siliciclastic rocks are low. Combined, these features indicate that the carbonate rocks of the KSF accumulated in a shallow lacustrine setting. Major types of carbonate facies were formed by: (1) biologically-induced precipitation; (2) evaporitic removal of CO_2 in a closed lake environment; and (3) chemical precipitation from thermal springs. Apparently, none of these carbonate facies was in full isotopic equilibrium with atmospheric CO_2. This interpretation shows the importance of taking into account the interplay between global and local depositional factors when interpreting the isotopic signature of the KSF dolostones and its implication for the Palaeoproterozoic carbon isotope excursion.

KEY WORDS: Alluvial, dolomite, evaporite, stromatolite, travertine.

Stratigraphic fluctuations in the stable carbon isotopic composition of Palaeoproterozoic sedimentary carbonates have attracted considerable interest, particularly because of their potential for monitoring global events and for chemostratigraphic correlations. In looking for stratigraphic and, hence, secular $\delta^{13}C_{carb}$ variations in Palaeoproterozoic sequences, it is important to be aware of processes and depositional environments which cause isotopic fractionation; for example, enrichment in ^{13}C might be caused not only by global factors, but is also known to be characteristic of some of local environments (e.g. Beauchamp *et al.* 1987).

In general, knowledge of sequence stratigraphy, palaeotectonic and depositional palaeoenvironments, as well as post-depositional conditions of Palaeoproterozoic ^{13}C-rich carbonates is very limited. Correlation between marine and non-marine environments from the 2330–2060 Ma time interval has not yet been made. There is an obvious difficulty in differentiating marine from lacustrine deposits in the Palaeoproterozoic because of the absence of fossils and diagnostic sedimentary structures. The distinction between marine and non-marine carbonates and evaporites is not trivial, and many ancient lacustrine carbonates and evaporites have been incorrectly identified as marine deposits (see the discussion in Smoot & Lowenstein 1991). Tidal sedimentary structures provide some of the best evidence of marine conditions in the Precambrian (Eriksson & Simpson 2000, 2002). However, these are not commonly preserved and are difficult to identify. The lack of well-documented data on Palaeoproterozoic depositional environments of ^{13}C-rich carbonates hampers the estimation as to what extent $\delta^{13}C$ has been affected by various local factors. This problem has been acknowledged in attempting to explain some extremely high $\delta^{13}C$ values as if they were of a global nature (Melezhik & Fallick 1996, 1997; Melezhik *et al.* 1997b, 1999, 2000).

In the present article, the authors consider carbonate rocks of the Palaeoproterozoic Kuetsjärvi Sedimentary Formation (KSF) exhibiting $\delta^{13}C$ values in the +6 to +8‰ range (Karhu 1993; Melezhik & Fallick 1996). The KSF was drilled in 1980s, among other formations, for the purpose of 'deep-mapping' the Palaeoproterozoic Pechenga Greenstone Belt, and establishing and describing the Jatulian para-stratotype sequence. Subsequently, drill core material has become available enabling detailed litho- and chemostratigraphic study. Consequently, the KSF succession is amongst the best-documented Palaeoproterozic successions in the world. The KSF was previously reported to have formed in shallow-water marine environments (Predovsky *et al.* 1974, p. 19; Negrutza 1984, pp. 170–171), and therefore, it has the potential to be used as one of the key sections in the reconstruction of the isotopic composition of Palaeoproterozoic sea water. The main objectives of this contribution are to: (1) present new sedimentological data; (2) argue that the entire Kuetsjärvi sequence accumulated in a deltaic and lacustrine setting; and (3) discuss the implications of the palaeoenvironmental data for the Palaeoproterozoic global isotopic shift of carbonate carbon.

1. Stratigraphy and age constraints

The KSF belongs to the Palaeoproterozoic Pechenga Greenstone Belt, Kola Peninsula, NW Russia (Fig. 1a). Structurally, the Pechenga Belt is composed of two subzones (Fig. 1b). The northern subzone is a simple half-graben filled with predominantly volcanic rocks gently dipping 10–40° southwards, whereas the southern subzone is a tectonically imbricated

https://doi.org/10.1017/S0263593300001140 Published online by Cambridge University Press

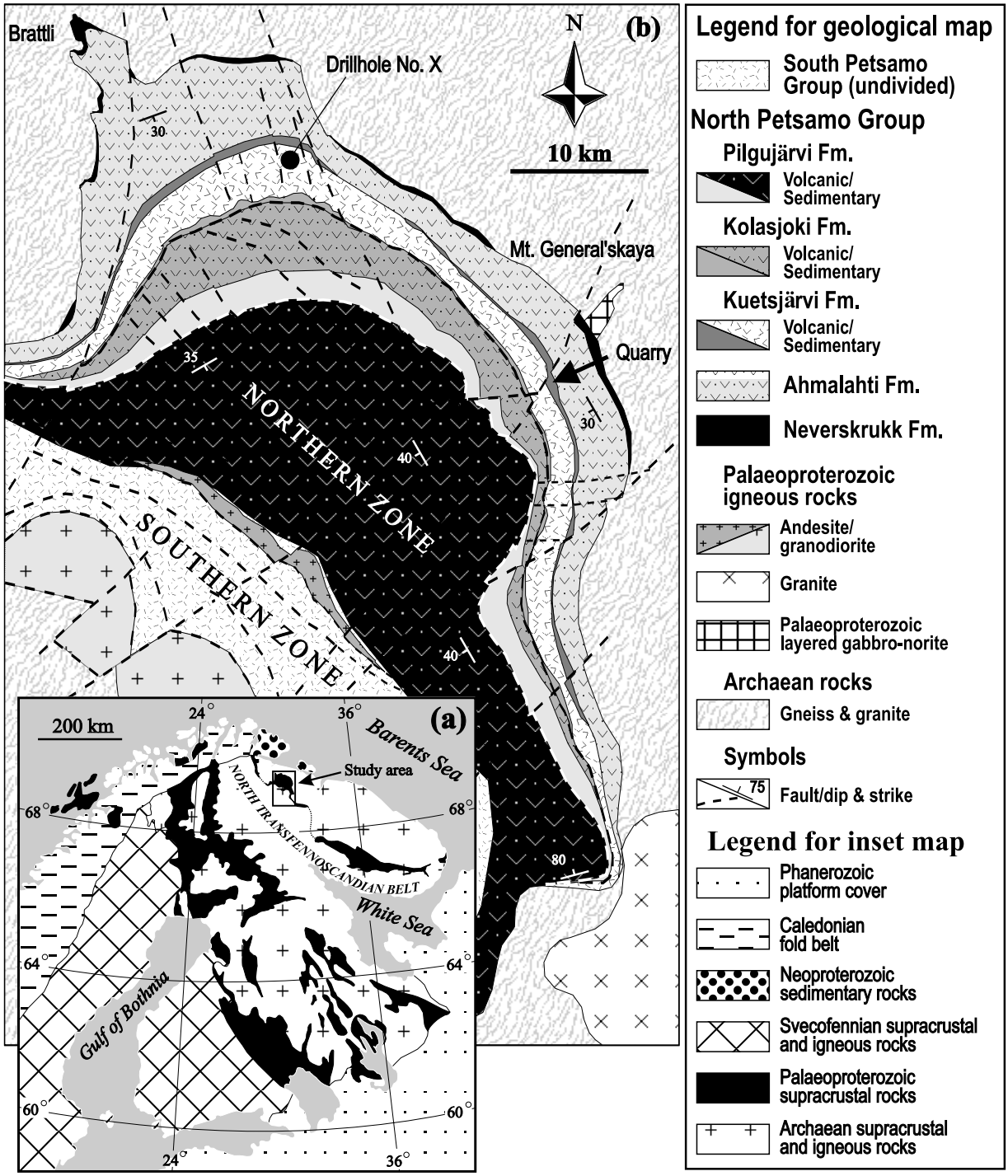

Figure 1 (a) Geographical and geological location of the study area (inset map) and (b) simplified geological map of the Pechenga Greenstone Belt (modified after Zagorodny *et al.* 1964). Positions of the studied drill hole and dolostone quarry are marked by the solid circle and arrow, respectively.

nappe overthrust by Archaean rocks (Fig. 1b). Within the northern half-graben, the thickness of the KSF varies considerably because of a series of transversal syndepositional faults and related small-scale grabens (Melezhik *et al.* 1994).

The rocks of the Pechenga Belt comprise the Petsamo Supergroup, which is subdivided into a lower, North Pechenga Group and an upper South Pechenga Group. The latter is not of concern here. The North Pechenga Group is composed of four paired sedimentary/volcanic cycles, each separated by either non-depositional unconformities or faults (Fig. 2). The unconformities are in places marked by palaeosols (Melezhik & Sturt 1994). The sedimentary and volcanic members are mutually transitional both vertically and laterally. Each pair begins with sedimentary rocks and ends with a thicker unit of mainly basaltic volcanic rocks. The cumulative stratigraphic thicknesses of the sedimentary and volcanic rocks are 1600 and 12 000 m, respectively. The rocks have undergone metamorphism from prehnite-pumpellyite to greenschist facies in the central part of the Pechenga Belt, and to amphibolite facies towards the peripheral zones (Petrov & Voloshina 1995). In general terms, the Pechenga–Pasvik Greenstone Belt is a Palaeoproterozoic long-lived (from 2500 to 1850 Ma) intracontinental rift developed into an intercontinental rift with a subsequent aborted oceanic phase (e.g. Marker 1985; Mints 1993; Melezhik & Sturt 1994; Sharkov & Smolkin 1997).

https://doi.org/10.1017/S0263593300001140 Published online by Cambridge University Press

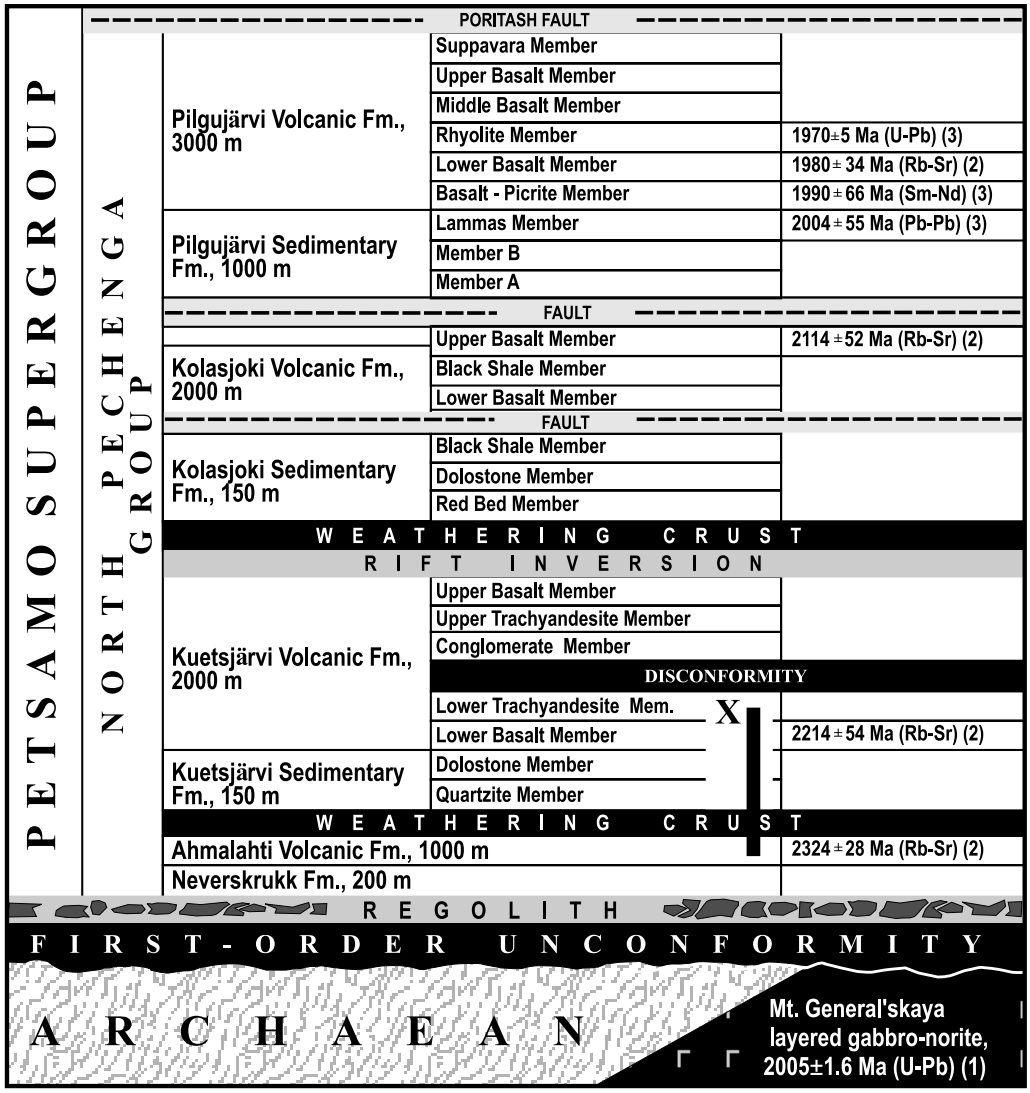

Figure 2 Stratigraphic section of the Pechenga Greenstone Belt, available radiometric ages and position of drill hole No. X (DHX). The formational stratigraphy is adapted from Zagorodny *et al.* (1964), with modification by Melezhik *et al.* (1995). Age data are from: (1) Amelin *et al.* (1995); (2) Balashov (1996); and (3) Hanski *et al.* (1990).

The lower age limit of the North Pechenga Group is constrained by the presence of gabbro-norite pebbles in the basal conglomerates (Bakushkin & Akhmedov 1975; Fig. 2). The pebbles are derived from the Mt. Generalskaya layered intrusion which has been dated to 2505 ± 1·6 Ma (Fig. 2; U-Pb-zircon; Amelin *et al.* 1995). The upper age limit of the group is younger than 1970 ± 5 Ma (U-Pb-zircon; Hanski *et al.* 1990) obtained from rhyolitic tuffs of the Pilgujärvi Volcanic Formation (Fig. 2). Thus, the age of the KSF can be bracketed between 2505 and 1970 Ma if U-Pb age determinations are used (Fig. 2).

There are two formations underlying the KSF. The lower Neverskrukk Formation rests unconformably and with well-developed regolith on Archaean basement (Sturt *et al.* 1994). It is composed of immature, closely packed, poorly sorted, framework-supported conglomerates which can be shown to have local sources. Depositional palaeoenvironments include alluvial channels and fans, in combination with shallow-water, ephemeral lakes (Melezhik 1992; Sturt *et al.* 1994). This fluviatile–lacustrine sequence is overlain by subaerially deposited amygdaloidal basalts, basaltic andesites and dacites of the Ahmalahti Volcanic Formation. The formation does not show any features suggesting deposition in a marine environment (Predovsky *et al.* 1974).

The KSF is a 15- to 150-m-thick unit that lies on the weathered basalts of the Ahmalahti Volcanic Formation (Predovsky *et al.* 1974). It consists of Quartzite and Dolostone Members (Fig. 2; Melezhik *et al.* 1994). The KSF is overlain with a gradational contact by the 50- to 2000-m-thick Kuetsjärvi Volcanic Formation consisting of subaerially erupted, trachybasalt, trachyandesite, mugearite and albitophyre (Predovsky *et al.* 1974). The volcanic sequence is composed of numerous, ubiquitously amygdaloidal volcanic flows with widely developed columnar joints. The flows are, in places, separated by thin layers of interflow breccia. Individual flows have dark-grey lower parts, and red or brownish upper parts. Contraction, exfoliation and reddened joints gave rise to a polygonal structure at the top of some flow units. The structure is of palaeoenvironmental significance because the reddening is interpreted to have been caused by surface oxidation, which is a common phenomenon affecting lavas extruded in subaerial environments beneath an oxygenated atmosphere. The reddening of the tops of the flows is evidence that such an atmosphere existed when the Kuetsjärvi Volcanic Formation was formed. Predovsky *et al.* (1987) described the Kuetsjärvi Volcanic Formation as a typical representative of intracontinental rift volcanites.

https://doi.org/10.1017/S0263593300001140 Published online by Cambridge University Press

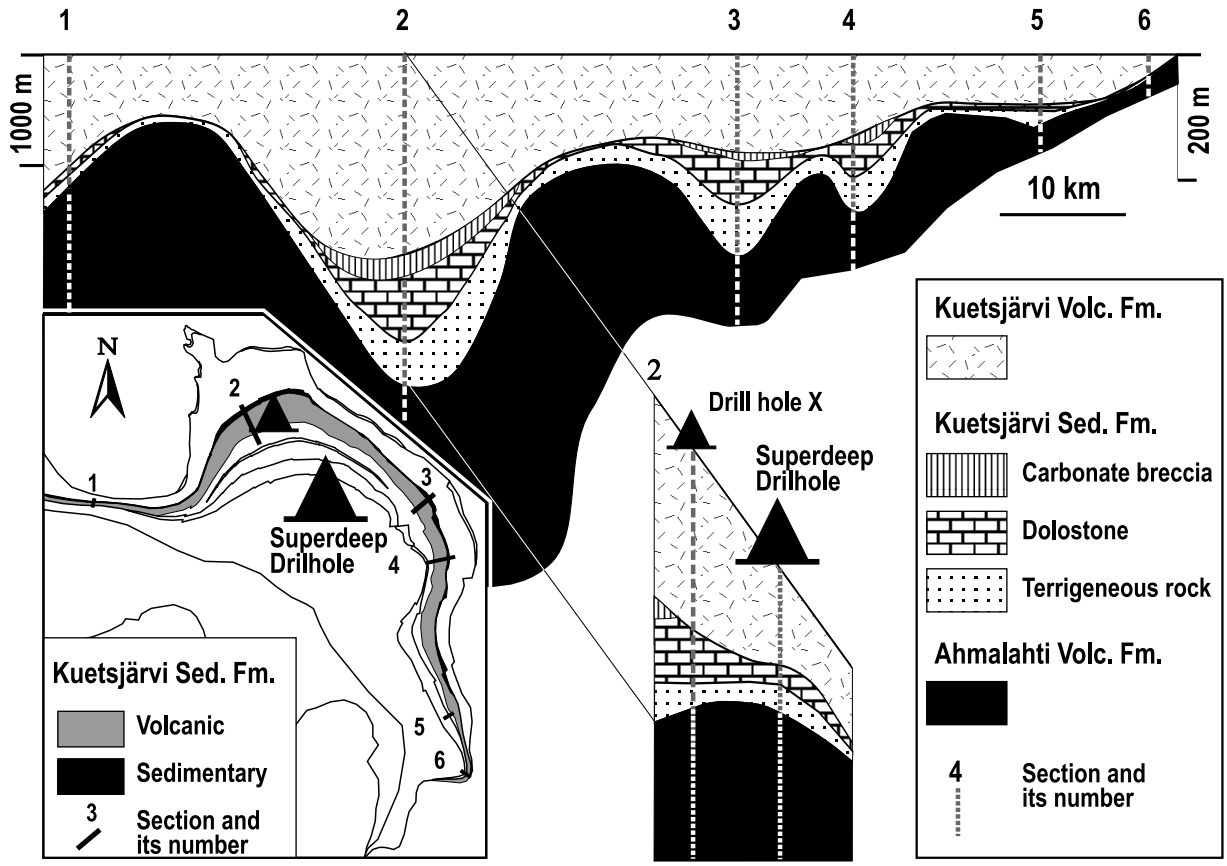

Figure 3 Three-dimensional lithological section of the Kuetsjärvi Sedimentary Formation based on natural exposures, quarries and drill holes, including the Kola Superdeep Drillhole. The vertical scale in the upper left upper corner is for volcanic rocks and the scale in the upper right corner is for sedimentary rocks. Note that vertical scales are exaggerated with respect to the horizontal scale.

2. Sampling sites

The drill core material of the KSF carbonate rocks has been recovered from the 1060-m-deep drill hole, No. X (DHX), from the central part of the Pechenga Belt (Fig. 1b). The drill hole intersected the entire c. 120-m-thick KSF, as well as parts of underlying and overlying volcanic units (Fig. 2). The present authors' contribution to sedimentary facies analysis is based on a combined study of drill core material and investigation of available outcrops in the vicinity of DHX. The low-grade greenschist facies metamorphism led to moderate recrystallisation of almost all the carbonate rocks which have been sampled. Therefore, the field observations of macroscopic structures and textures of carbonate rocks cannot always be supported by petrographic study.

3. Analytical techniques

Fe_2O_3, FeO and CO_2 were determined by wet chemistry. Other major as well as trace elements were analysed by X-ray fluorescence spectrometry at the Geological Survey of Norway, Trondheim (NGU) using a Philips PW 1480 X-ray spectrometer. The accuracy (1σ) is typically better than 2% of the oxide present (SiO_2, Al_2O_3, $Fe_2O_{3(tot)}$, MgO, CaO, Na_2O, or K_2O), even at the level of 0·05 wt%, and the precision is almost invariably higher than the accuracy. The analytical uncertainty (1σ) for MnO is better than ± 0·01%.

Acid-soluble CaO, MgO and MnO were analysed by inductively coupled plasma atomic emission spectrometry (ICP-AES) at NGU using a Thermo Jarrell Ash ICP 61 instrument. The detection limits for MgO, CaO and MnO are 100, 200 and 0·2 ppm, respectively. The total analytical uncertainty including element extraction (1σ) is ± 10% rel.

Standard analytical procedures were used for the measurement of organic carbon at the Geological Institute in Apatity, Russia. Organic carbon content was measured from acid-washed material via sealed tube combustion.

4. Three-dimensional variations of lithofacies and thicknesses of the KSF

A three-dimensional section based on the drill holes, including the Kola Superdeep Drillhole, shows that the thickness of the KSF varies considerably (Fig. 3; largely because of syndepositional faults and small-scale grabens; Melezhik *et al.* 1994). The greatest thickness is recorded in the central part of the Pechenga Belt where the formation is intersected by DHX. Here, the thickness of siliciclastic rocks (Quartzite Member) is three times greater than in other parts of the belt. The maximal thicknesses of the Dolostone Member (60–80 m) occur in three sub-basins (Fig. 3). The tuff-cemented dolostone breccia, terminating the Dolostone Member, has only been recorded in the central part of the belt. In other places, the breccia is missing and basaltic tuff overlies the Dolostone Member (Figs 1 & 2).

5. Description and interpretation of stratigraphic section of the KSF

In general, the KSF consists of siliciclastic-dominated, mixed siliciclastic–dolostone and dolostone-dominated parts with upwards-increasing dolostone content at the expense of siliciclastic rocks. The differentiated units are numbered from I to

https://doi.org/10.1017/S0263593300001140 Published online by Cambridge University Press

XI, starting from the lower part of the sequence (Fig. 4). Characteristics of the units are given in the text and in Tables 1 and 2. Sedimentological features of the main rock types are illustrated by photographs.

5.1. Palaeosol (Unit I)

5.1.1. Observations. Unweathered amygdaloidal basaltic andesites underlying the KSF (Fig. 4) are geochemically homogeneous rocks (Predovsky *et al*. 1974, 1987; Skuf'in 1993). Their average composition is shown in Table 3 and plotted on geochemical profiles (Fig. 5). However, from the contact with the KSF downward for as much as 2 m, these volcanic rocks are sericitised, calcitised and chloritised. Three alteration zones have been recognised (Fig. 5). The c. 1-m-thick lower zone is characterised by moderate sericitisation and calcitisation of albite, and chloritisation and biotitisation of actinolite. This leads to oxidation of Fe and depletion of rocks in SiO_2, Al_2O_3 and CaO, as compared to the unaltered variety (Table 3). The K_2O/Na_2O and Fe_2O_3/FeO ratios are 3·7 and 1·3, respectively, compared to 0·4 and 0·6 in the unaltered rocks. Primary ophitic texture can easily be recognised. The second zone is less than 0·5-m-thick. It has a transitional contact with the underlying zone and is marked by a very intensive replacement of albite by calcite and sericite. The calcite is both replacive and displacive. Amphibole is entirely replaced by biotite and chlorite. The Fe_2O_3/FeO remains unchanged, whereas K_2O/Na_2O >50. Ophitic texture is not preserved. The third zone, only 0·3-m-thick, consists of biotite, sericite, chlorite, dolomite, calcite with subordinate quartz, talc and serpentine. The calcite is mainly displacive. These rocks have a lensoidal structure and markedly high concentration of non-carbonate MgO ranging from 7·5% to 20%, and K_2O/Na_2O fluctuating between 90 and 340.

5.1.2. Interpretation. Geochemical and petrographic data and the position of the altered rocks are most consistent with weathering processes which occurred prior to deposition of the KSF. The first and second zones represent part of an ancient weathering crust (i.e. a palaeoregolith). Since the rocks in these two zones are not marked by elevated Al_2O_3 concentration, the present authors interpret them to represent a low part of the weathering profile. The upper part is considered to have been removed and might have been partly incorporated into the third zone, which is interpreted as a redeposited crust of weathering. Incorporation of foreign clasts into the redeposited material resulted in an only slightly elevated Al_2O_3 concentration in the redeposited crust. Nevertheless, the weathering profile is conspicuous as it is highly enriched in calcite. The latter is both replacive and displacive, and exhibits some similarities with caliche developed elsewhere in basalts (e.g. Capo *et al*. 2000; Knauth *et al*. 2003).

5.2. Quartzite Member

5.2.1. Mixed siliciclastic-dolostone Unit II. This unit is 12·6-m-thick and defines the lowermost part of the KSF (Fig. 4, Table 1). It starts with a drab, fine-grained, arkosic sandstone and siltstone interbedded with thin layers of dark sericitic mudstone. The basal unit is characterised by a highly disrupted structure of horizontally laminated mudstones which involves soft sediment deformation, development of flame and different kinds of loading structures (Fig. 6a). This is followed by interbedded fine-grained sandstone, siltstone and subordinate mudstone characterised by a high sandstone/siltstone to mudstone ratio. These rocks are typified by thin (1–5 cm), graded (Bouma sequences) sand-silt layers (Fig. 6b–d). Common features include centimetre-scale, ripple cross- and low-angle-flat laminations (Fig. 6b–d, f), and fining-upward from scoured, erosive bases (Fig. 6b). Ripples are asymmetric with low relief of 0·2–0·5 cm, wavelengths of 1–5 cm and display unidirectional migration (Fig. 6e). Soft-sediment deformation, small-scale slump structures (Fig. 6b) and mud chips incorporated into sandy layers (Fig. 6c) are also present.

The upper part of Unit II consists of arkosic siltstones and dolomite-cemented sandstones interbedded with thin layers of dolostone, intraformational dolostone breccia (Fig. 6g), and flat-pebble, matrix-supported, dolostone conglomerate (Fig. 6h). The dolostone layers have limited areal extent and represent short-lived features. Some dolostone beds have been split up by planar cracks parallel to the bedding into several sheets resulting in complex, brecciated cross-sections (Fig. 6g). Both vertical and sheet crack infills are composed of clayey sandstone as well as dolostone debris spalled off crack walls. Mudstone layers, where present, are generally thin with a low lateral continuity and some show probable desiccation cracks (Fig. 6i). The most common sedimentary structures are well-developed, parallel sand and silt laminations showing graded bedding with rare, small-scale, unidirectional, ripple cross-lamination. Slump horizons occur in places (Fig. 7a). The bases of beds commonly exhibit numerous small scour-and-fill structures (Fig. 7b), and locally, larger channels (Fig. 7c). The scours are filled with fine-grained sandstone grading into siltstone (Fig. 7b), whereas the larger channels are composed of either poorly sorted dolarenite (Fig. 7c) or matrix-supported, flat-pebble conglomerates where tabular fragments of micritic dolostone are emplaced in silty, dolomite-cemented, quartz matrix. In places, starved, unidirectional, current ripples are developed (Fig. 7d).

The dolostones are commonly pink, both micritic and allochemical, undulose-bedded, comprising 1–5-cm-thick beds with transitional lower, and sharp erosive upper contact (Fig. 7e). Some beds are associated with thin layers of mudstones. A few beds exhibit fine undulatory lamination, thus resembling stromatolites. The dolostone beds contain several internal erosional surfaces, and in places, spherical or polygonal inclusions of dolomite resembling pseudomorphed sulphate nodules (Fig. 7f).

5.2.2. Siliciclastic-dominated Unit III. Unit III (Fig. 4, Table 1) is 17·5-m-thick, and its lower part is composed of pink, purple and brown, fine-grained, haematite-rich, arkosic sandstones with subordinate thin layers of sericite-rich mudstones. These rocks typically appear structureless, but rare decimetre-scale trough cross-lamination, horizontally laminated sandstone–mudstone interbeds and small-scale, soft-sediment deformations, including ball-and-pillow structures, can be observed (Figs. 8a, b).

The upper part of Unit III is composed of brown sandstone that also appears structureless, but in places, contains abundant highly deformed, dismembered, randomly oriented, black, haematite-rich, mudstone layers with flame structure. Locally, the pink and purple sandstone has been subject to intensive post-sedimentary (catagenetic) discoloration that resulted in partial overprint of the primary colour, lamination and bedding (Fig. 8c).

5.2.3. Mixed siliciclastic-dolostone Unit IV. This unit is c. 10 m thick (Fig. 4, Table 1). Its lower part is composed of pink, brown, violet and purple siltstones (Fig. 8d–g), and subordinate, haematite-rich mudstones with minor sandy limestone and dolostone, whereas the upper part is marked by pink and violet, haematite-rich, and pale green arkosic sandstones and siltstones. The grain size increases from <0·001–0·01 to 0·02–0·8 mm from the lower to the upper part of the unit (Table 4). Overall, the unit is distinguished by thin horizontal, varve-like lamination (Fig. 8d–g). The red colour of the rocks is caused by the presence of haematite particles, whereas

https://doi.org/10.1017/S0263593300001140 Published online by Cambridge University Press

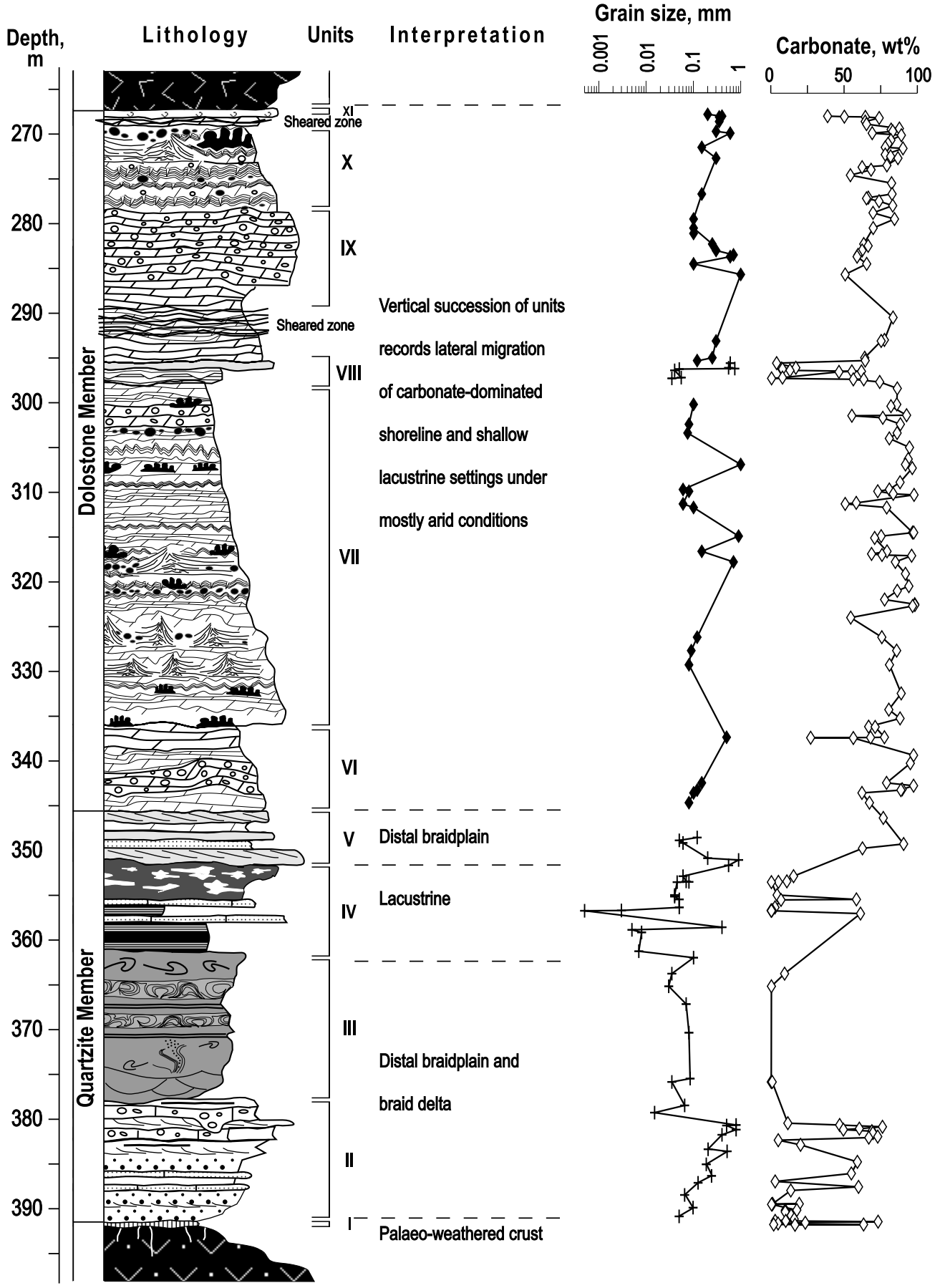

lighter colours are a result of intensive 'bleaching' and discolouration, yielding a 'mottled' (Fig. 8f) and variegated (Fig. 8g) appearance.

5.2.4. Mixed siliciclastic-dolostone Unit V. Unit V is 5·7-m-thick and occurs at the top of the Quartzite Member (Figs. 2 & 4, Table 1). It consists of interbedded quartzitic sandstones,

https://doi.org/10.1017/S0263593300001140 Published online by Cambridge University Press

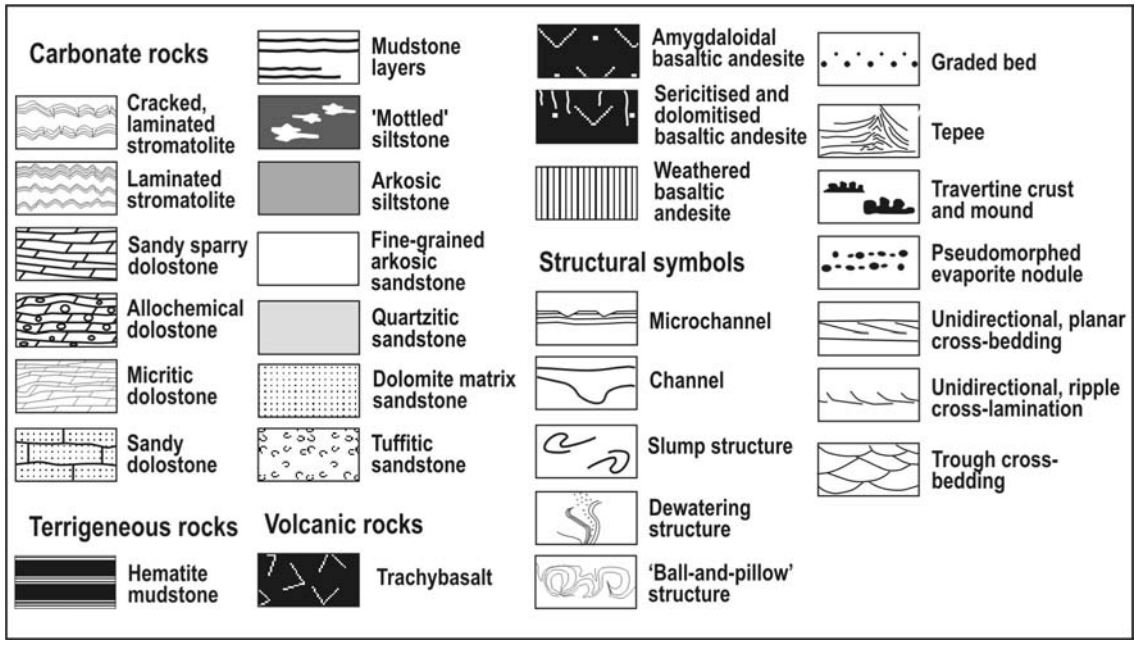

Figure 4 Variation of lithofacies, size of quartz and feldspar grains (crosses for siliciclastic and diamonds for carbonate rock), and content of carbonate material in the stratigraphic column of the Kuetsjärvi Sedimentary Formation.

dolostone-cemented arkosic sandstones and thin beds of sandy dolostones. Although the rocks are in various proportions, the quartz sandstones are the dominant lithology. The sandstones are characterised by unidirectional planar cross-bedding (Fig. 8h, i); other rocks are either massive or show indistinct, crude, horizontal bedding.

5.3. Palaeoenvironmental interpretation of Quartzite Member, Units II–V

Unit II represents an overall coarsening-upwards sequence (Fig. 4, Tables 1 & 4), which is, in general, a typical feature of deltaic and lake margin sequences (Miall 1984; Elliot 1986; Smoot 1991; Reading & Collinson 1996). The thinly laminated mudstones of the basal part of the sequence can be interpreted as sediments accumulated in a standing body of water which developed to cover the underlying palaeoweathering crust. Abundant soft-sediment deformation and loading features can be attributed to the rapid deposition of fine-grained sand and silt on unconsolidated mud as a result of progradation or switching of braid deltas/braid plains along the shoreline.

The sedimentological features of the lower part of Unit II, such as thin, graded sand-silt layers, centimetre-scale, unidirectional ripple cross-lamination and normally graded sandstone capped with mudstone (Fig. 6g, i) represent deposition by turbidity currents and suspension fallout. Unidirectional cross-lamination is interpreted as the deposition product of migrating ripples under unidirectional, low-flow-regime conditions (e.g. Miall 1977). Asymmetrical ripple marks attest to unidirectional current, and the small wavelength and amplitude of the ripple bedforms suggest deposition in shallow water (Tucker 1978; Martel & Gibling 1991). Small-scale slumps are indicative of subaqueous, small-scale, gravity-induced mass movement caused by high depositional rates, which is a common process along shoreline 'delta front' environments (Reineck & Singh 1980; Coleman & Prior 1982; Miall 1984; Elliott 1986; Reading & Collinson 1996).

The upper part of Unit II is marked by numerous thin, discontinuous, desiccated mudstone layers associated with thin, commonly desiccated and *in situ* brecciated beds of sandy dolostones. The angular blocks in breccia-like fabrics (Fig. 6g) indicate old lake/pond bottom that has been disrupted by repeated wetting and drying (Smoot 1991). Such association is commonly found in shallow water shoreline settings and in interdistributary basins in the delta plain (e.g. Elliott 1986; Reading & Collinson 1996). These features in close spatial association with other mudstone, dolostone and carbonate breccias suggest that the carbonate precipitation took place in shallow-water and ephemeral ponds. Beds of massive micritic dolomite might have formed by evaporative removal of CO_2. This is a typical feature of semi-arid sandflat–mudflat marginal lacustrine facies (Szulc *et al*. 1991). The semi-arid climate is supported by the presence of dolomite-pseudomorphed micronodules of apparent sulphates in layers of micritic dolostones. An arid climate is also consistent with a low degree of weathering of feldspar clasts (Table 4). Carbonates comprising the flat-laminated stromatolitic 'mats' are interpreted as biologically induced precipitates. Such carbonates are rather common in many shallow-water and playa lakes, and isolated ponds on shorelines and fluvial planes (e.g. McBride *et al*. 1973; Horton & Schmitt 1996; Camoin *et al*. 1997). In addition, the association of desiccated mud layers, *in situ* brecciated dolostone beds and superficial dolocrete suggests that pedogenesis occurred (Melezhik *et al*. 2004). Calcrete is common in many shoreline settings (Freytet 1973; McBride *et al* 1973; Elliott 1986; Coleman & Prior 1982).

Finer-grained Unit III replaces abruptly the coarser Unit II lithologies (Fig. 4, Table 4). The overall observed sedimentological features of Unit III (Table 1), such as a thick body of fine-grained sandstone having a relative lack of sedimentary structures, and sandstones with soft-sediment deformation, slump and 'ball-and-pillow' structures (Fig. 8a), are most consistent with the influx of fluvial sediment to the shoreline (Hyne *et al*. 1979; Miall 1984; Elliott 1986), i.e. a fine-grained braid delta (McPherson *et al*. 1987). Massive sandstone is attributed to rapid deposition by subaqueous, high-density turbidity currents (e.g. Lowe 1982; Chough *et al*. 1990; Higgs 1990) from turbulent suspension with insufficient time for bedform development (e.g. Lowe 1982). The 'ball-and-pillow' structures (Fig. 8a) were apparently caused by

https://doi.org/10.1017/S0263593300001140 Published online by Cambridge University Press

Table 1 Lithological characteristics of the clastic–dominated and mixed clastic-dolostone units of the Kuetsjärvi Sedimentary Formation (drill hole X)

Unit	Interval (m)	Lithology	Colour	Sedimentary features	Clast size (mm)	Clast composition/ authigenic mineral	Matrix	Depositional setting
Unit XI*	267·8–268·05	Sandy dolostone and tuffogenic sandstone interbeds, intraformational dolostone breccia	Green	Discontinuous beds	0·1–0·3	Rounded and angular quartz/pyrite	Chlorite, quartz	Subaerially exposed carbonate shoreline influenced by subaerial volcanism
Unit VIII*	295·5–297·7	Interbedded dolomite breccia and sericite-chlorite mudstone; coarse-grained quartzitic sandstone	Drab, greenish-grey	Discontinuous beds laterally variable in thickness; fine planar lamination, micro cross-lamination; scours	Mudstone: 0·03–0·06; sandstone: 0·4–1·0	Mudstone: angular grains of quartz, microcline; tourmaline/pyrite; sandstone: well-rounded quartz/pyrite	Sericite, chlorite, dolomite	Subaerially exposed carbonate shoreline
Unit V*	345·5–351·2	Interbedded fine- to coarse-grained, dolomite-cemented quartzitic and arkosic sandstone; sandy, micritic and sparry allochemical dolostone	Drab, pale grey	Discontinuous beds laterally variable in thickness; crude horizontal and planar, unidirectional cross-stratification	0·04–1·2	Quartz, microcline, muscovite; zircon, tourmaline/apatite, tourmaline	Calcite, sericite	Distal braidplain
Unit IV	351·2–361·3	'Mottled' fine-grained siltstone; haematite-rich, sericitic mudstone; subordinate sandy, sparry, dolostone and limestone	Brown, purple, green; violet with patches of brown, pink and beige	Laterally continuous beds of equal and uniform thickness, fine-scale planar; varve-like fine lamination	<0·001–0·08	Quartz, microcline, plagioclase, tourmaline; abundant particles of haematite (0·005–0·02 mm)/tourmaline, apatite	Sericite, calcite	Lacustrine
Unit III	361·3–378·8	Fine-grained, haematite-bearing, sandstone; subordinate sericitic mudstone	Pink, brown, flieder-farben	Laterally continuous beds of unequal and variable thickness; small-scale trough cross-lamination; abundant soft-sediment deformation features ('ball-and-pillow', fluid-escape and slumps)	0·02–0·15	Quartz, microcline, plagioclase, haematite, tourmaline; abundant particles of clastic haematite (0·01–0·4 mm)	Sericite, quartz	Braid-delta front
Unit II*	378·8–391·5	Interbedded fine- to coarse-grained arkosic sandstone and sericitic mudstone; thin lenses of sandy, micritic dolostone and micritic, allochemical dolostone; sporadic lenses of flat-pebble conglomerate	Drab, dark grey, pale grey	Coarsening-upwards sequence; discontinuous beds unequal and laterally variable in thickness; abundant graded bedding; thin planar lamination, unidirectional small-scale, low angle, planar and trough, cross-lamination; starved sand ripples, slumps; soft-sediment deformation; thinly laminated, desiccated, mudstone; fining-upwards scours	Sandstones: 0·05–1·0; breccias: 5–120	Quartz, muscovite microcline, biotite, dark tourmaline, plagioclase, fragments of micritic dolostones/light-green tourmaline, calcite and dolomite	Sericite, quartz, dolomite	Siliciclastic-dominated inter-distributary shoreline
Unit I (palaeo-weathered crust)	391·5–391·8	Dolomitised phlogopite-chlorite-sericite schist	Dark grey, white	Locally developed lenses, transitional contact with underlying basaltic andesite	–	–	–	Calichified palaeo-weathered crust

*Interbedded carbonate rocks are characterised in Table 2.

Table 2 Lithological characteristics of mixed clastic-dolostone and dolostone-dominated units of the Kuetsjärvi Sedimentary Formation (drill hole X)

Unit	Interval (m)	Lithology	Colour	Sedimentary features	Allochem	Allochem size	Matrix	Depositional setting
Unit XI*	267·8–268·05	Sandy dolostone and tuffogenic sandstone interbeds, intraformational dolostone breccia	Grey, green	Discontinuous beds	–	–	Coarsely crystalline dolomite, 200–300 μm	Subaerially exposed carbonate shoreline influenced by subaerial volcanism
Unit X	268·8–278·0	Interbedded algal micritic dolostone, sandy sparry allochemical dolostone and micritic dolostone; abundant travertine; dolomite-pseudomorphed micronodules (1–5 mm) of probable sulphates; silcrete, dolocrete	Pink	Laterally continuous beds of unequal and variable thickness; fine microbial lamination, planar lamination; abundant tepee structures; and associated brecciation and buckling; abundant surface dissolution cavities	Rounded and platy, unsorted intraclasts of micritic and algal dolostones, 0·1–4 cm in size	Dolorudite	Cryptocrystalline to coarsely crystalline dolomite, <4–100 μm	Carbonate shoreline influenced by hydrothermal springs in a shallow-water, playa-like, lacustrine setting; semi-arid climate
Unit IX	278·0–287·0	Sandy, sparry, allochemical dolostone	Pale grey	Laterally continuous beds of unequal and variable thickness; crude cross-lamination; scoured surfaces	Rounded intraclasts of micritic dolostones	Dolorudite	Medium to coarsely crystalline dolomite, 40–100 μm	Subaerially exposed carbonate shoreline
Shear zone rocks	268·05–268·8; 287·0–295·5	Sparry and micritic, sandy dolostone	Dark pink, brown, drab	–	–	–	Cryptocrystalline to coarsely crystalline dolomite, <4–200 μm	?
Unit VIII*	296·2–297·7	Interbedded dolomite breccia and sericite-chlorite mudstone; coarse-grained quartzitic sandstone	Drab, pink	Discontinuous beds with crude planar stratification	Angular and partly rounded clasts of recrystallised dolostones	Dolorudite	Very coarsely crystalline dolomite	Subaerially exposed carbonate shoreline
Unit VII	297·7–336·0	Interbedded algal micritic dolostone, sandy micritic allochemical dolostone, subordinate sandy sparry dolostone; travertine crust, dolocrete, silcrete; probable gypsum nodules replaced by dolomite; authigenic albite	Pale grey, white	Laterally continuous beds of unequal and variable thickness; fine microbial lamination, fine planar lamination, cross-lamination; small-scale tepee structure, channels, scoured surfaces, fenestrae, brecciation and buckling	Rounded and angular intraclasts of micritic dolostone and algal micritic dolostone	Dolorudite	Very finely to finely crystalline dolomite, 6–20 μm	Carbonate-dominated coastal plain occasionally influenced by hydrothermal springs in shallow-water, playa-like, lacustrine setting; arid climate
Unit VI	336·0–345·5	Interbedded sandy sparry dolostone, sandy micritic dolostone and subordinate sandy sparry allochemical dolostone	White, pale grey	Laterally continuous beds of unequal and variable thickness ('pinch-and-swell' bedding); massive, planar- and cross-laminated; relicts of microbial laminae	Rounded, sorted intraclasts of micritic allochemical dolostone; quartz, plates of micritic dolostone	Dolorudite	Very finely to very coarsely crystalline dolomite, 10 μm to 4 mm	Carbonate plain in shallow-water, low-energy setting
Unit V*	345·5–351·2	Interbedded fine- to coarse-grained, dolomite-cemented arkosic and quartz sandstone, sandy micritic dolostone and sparry allochemical dolostone	White	Discontinuous beds unequal and laterally variable in thickness (0·8–1·2 m); massive or crude planar bedding	Rounded and angular, unsorted intraclasts of micritic dolostone; rounded, unsorted grains of quartz and muscovite flakes	Dolorudite, dolarenite	Finely to very finely crystalline dolomite, 8–20 μm	Ephemeral ponds, braidplain
Unit II*	378·8–387·8	Interbedded sandy, micritic allochemical dolostone, arkosic sandstone, subordinate sericitic mudstone and flat pebble conglomerate	Pale grey, white, pink	Discontinuous, thin lenses with probable dolomite-pseudomorphed gypsum nodules; abundant *in situ* brecciation; erosional surfaces and scours	Unsorted plates of micritic dolostone; rounded, unsorted quartz grains and muscovite flakes, 0·1–1·0 mm in size	Dolorudite, dolarenite	Finely to coarsely crystalline dolomite, 10–500 μm	Interdistributary areas of braid delta; arid, semi-arid climate

*Interbedded terrigeneous rocks are characterised in Table 1.

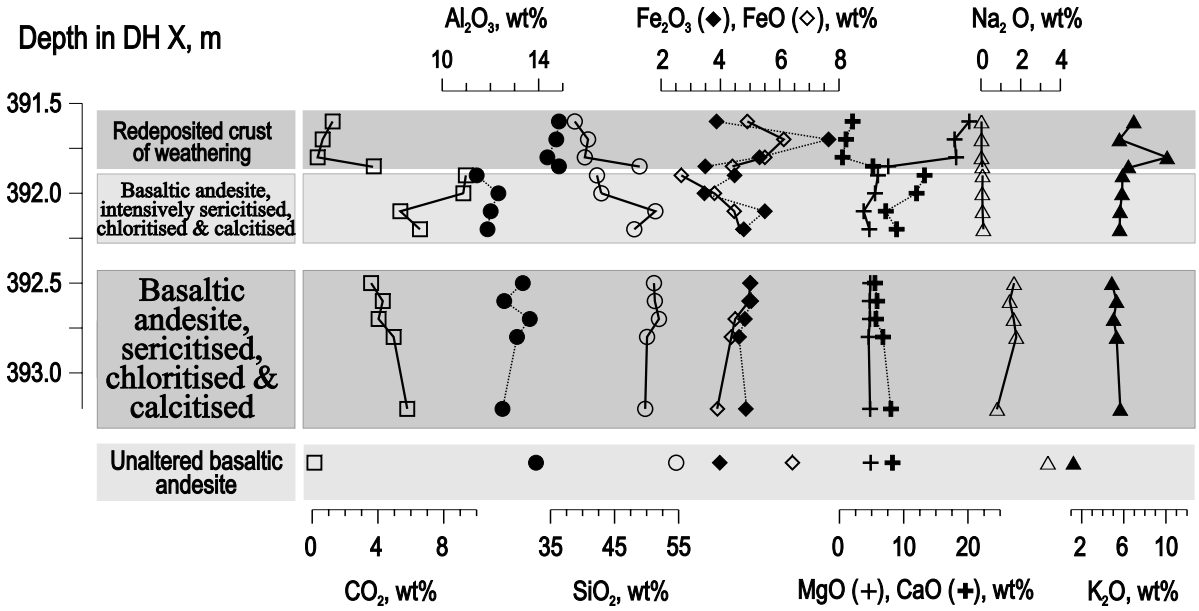

Figure 5 Geochemical profile through the palaeo-weathered basaltic andesites in the core of the Ahmalahti Volcanic Formation sampled beneath the Kuetsjärvi Sedimentary Formation. Drill hole depth is indicated from the surface.

Table 3 Chemical characteristics of weathered Ahmalahti basaltic andesite and redeposited weathering crust at the base of the Kuetsjärvi Sedimentary Formation (wt.%): (–) below detection limit of 0·01% for S_{tot} and 0·1% for C_{org}; and (n.d.) not determined

Sample number	Lithology	SiO_2	TiO_2	Al_2O_3	Fe_2O_3	FeO	MnO	MgO	CaO	Na_2O	K_2O	H_2O+	H_2O-	CO_2	P_2O_5	C_{org}	S_{tot}
Redeposited crust of weathering (Unit I)																	
391·6	Biotite–sericite–dolomite schist	38·7	0·89	14·8	3·87	4·91	0·17	20·2	2·05	0·03	6·96	5·51	0·35	1·24	0·20	n.d.	0·02
391·7	Biotite–sericite schist	40·8	0·74	14·7	7·65	6·14	0·05	17·9	1·03	0·03	5·59	3·72	0·19	0·63	0·18	–	0·06
391·8	Sericite–biotite schist	40·3	0·88	14·3	5·32	5·50	0·05	18·1	0·48	0·03	10·12	4·04	0·28	0·33	0·19	–	–
391·85	Sericite–dolomite schist	48·8	0·85	14·8	3·49	4·41	0·05	7·59	5·22	0·07	6·44	3·50	0·46	3·74	0·17	n.d.	–
Basaltic andesite, sericitised and intensively calcitised																	
391·9		42·2	0·64	11·4	4·48	2·68	0·11	5·99	13·2	0·08	5·88	3·53	0·64	9·34	0·12	n.d.	0·01
392·0		42·9	0·69	12·3	3·46	3·80	0·11	5·53	12·0	0·07	5·84	3·22	0·25	9·19	0·15	–	–
392·1		51·3	0·74	12·0	5·50	4·47	0·06	3·76	7·21	0·08	5·65	3·07	0·67	5·36	0·12	n.d.	–
392·2		48·0	0·71	11·8	4·79	4·66	0·09	4·65	8·90	0·12	5·61	3·14	0·53	6·55	0·12	n.d.	0·01
Basaltic andesite, sericitised and calcitised																	
392·5		51·1	0·78	13·3	5·02	5·00	0·10	4·79	5·54	1·67	4·87	3·67	0·55	3·58	0·13	–	–
392·6		51·2	0·72	12·5	5·04	4·97	0·10	4·72	5·87	1·45	5·32	3·12	0·63	4·29	0·11	n.d.	0·01
392·7		51·9	0·37	13·6	4·83	4·50	0·09	4·74	5·69	1·65	5·04	2·77	0·34	4·03	0·13	n.d.	–
392·8		50·0	0·72	13·1	4·63	4·37	0·10	4·54	6·77	1·78	5·32	2·99	0·57	4·95	0·14	n.d.	0·06
393·2		49·7	0·69	12·5	4·86	3·90	0·09	4·78	8·02	0·82	5·67	2·84	0·54	5·78	0·14	n.d.	0·02
395·5		53·5	0·59	12·2	6·76	2·58	0·12	2·56	11·0	1·45	3·73	2·76	0·32	2·63	0·08	–	0·04
*Basaltic andesite, unaltered**		54·6	0·92	13·8	3·98	6·43	0·16	4·86	8·26	3·38	1·23	1·81	0·16	0·13	0·11	n.d.	0·08

*Average composition of unaltered basaltic andesite (Predovsky *et al.* 1974, 1987).

water escape from non-consolidated sediments caused by a high depositional rate. Abundant, soft-sediment-deformed, dismembered fragments of haematite-rich mudstone beds in the uppermost massive sandstone and the presence of slump blocks are characteristic features of such settings (Coleman & Prior 1982; Miall 1984; Elliott 1986; Smoot 1991; Reading & Collinson 1996). Enrichment in haematite suggests an oxygenated depositional environment.

Varve-like, fine-grained sandstone-siltstone interbeds of Unit IV (Fig. 8d–g) most likely represent sediments deposited in a standing body of water. Such flat, continuous lamination has been reported from several Recent (Muchane 1996; Talbot & Allen 1996) and ancient lacustrine settings (Castle 1990; Smoot 1991). Therefore, the homogeneous character (Table 1) of Unit IV (Fig. 4), together with the well-sorted and rounded nature of clastic grains (Table 4), and varve-like lamination, are consistent with a shallow-water, low-energy, depositional setting, i.e. lacustrine. Enrichment in haematite and syn-depositional red coloration of the rocks (Melezhik 1992) suggests an oxygenated environment. Thus, Unit IV sediments suggest that the braided delta was either abandoned or switched to a different site.

Unit V sandstones with unidirectional, planar cross-stratification (Fig. 8h, i) suggest a return of a distal-braided, low-energy, fluvial system over the lacustrine and shoreline settings. The formation of carbonates implies either biologically driven chemical or purely chemical precipitation. Cementation of the alluvial sand by calcite and dolomite is interpreted

https://doi.org/10.1017/S0263593300001140 Published online by Cambridge University Press

as having a pedogenic origin (e.g. Freytet 1973; McBride *et al.* 1973; Elliott 1986; Coleman & Prior 1982; Horton & Schmitt 1996; Atabey *et al.* 1998).

Overall, the siliciclastic lithofacies lack tidal indicators, and several are marked by a red colour which seems to be the result of syn-depositional alteration of the rocks (e.g. oxidation under subaerial conditions). The KSF rocks, together with the Lower Jatulian sequences of the Fennoscandian Shield, have been described in the literature as a classic example of Palaeoproterozoic 'red beds' (Predovsky *et al.* 1974; Sochava 1979; Melezhik 1992). Post-depositional alteration of Unit IV 'red beds', when present, is expressed by bleaching, discoloration and removal or reduction of oxidised iron by H_2S-free reducing solutions (Melezhik 1992). In general, a striking contrast in colour has been found between aqueous and terrestrial sediments (Shinn 1983; Southgate 1986). This is largely caused by the oxidation state of iron and the oxidation of organic matter. Green, red and purple colours, as well as mottling, have been reported to be a characteristic feature of many lacustrine and lacustrine delta deposits (McBride *et al.* 1973; McBride 1974; Glover & O'Beirne 1994; Olsen *et al.* 1996; Gierlowski-Kordesch 1998).

Consequently, based on the lines of evidence outlined above, the siliciclastic lithofacies of the Quartzite Member are interpreted to have formed in the braid-delta, shoreline and shallow-water settings of an oxygenated lake.

5.4. Dolostone Member

5.4.1. Dolostone-dominated Unit VI. Unit VI is 9·5 m thick and forms the lowermost dolostone-dominated part of KSF (Fig. 4). It consists of sparry, micritic and allochemical dolostones (Table 2) and although the sparry dolostones typify the upper part and the allochemical dolostones the middle part of the unit (Fig. 4), both lithologies have been observed to be mutually interbedded within a half-metre-scale core specimen. This alternation may also include 2- to 5-cm-thick layers of quartzitic sandstone (Fig. 9a). The sandy, sparry and micritic dolostones are characterised by fine (millimetre-scale) lamination, whereas the allochemical dolostones show thicker (centimetre-scale) horizontal lamination and planar cross-bedding. The allochemical dolostones contain rounded, sorted clasts and/or angular, unsorted plates of micritic dolostones. Microcrystalline, micritic dolostones contain relics of algal laminae composing millimetre-scale films, or forming encrustations.

5.4.2. Dolostone-dominated Unit VII. Unit VII is the thickest (38·3 m) dolostone-dominated unit in the formation (Fig. 4, Table 2). It consists of interbedded white, algal, micritic dolostones, and silty to sandy, allochemical dolostones and abundant travertine crusts (Melezhik & Fallick 2001). Sandy, micritic, allochemical dolostones, and sandy, sparry and massive, micritic dolostones occur in subordinate proportions. There are several intervals where dolostones were affected by tectonic shearing, which is accompanied by the formation of chlorite veinlets.

Although only flat-laminated stromatolites have been documented in the core material (Fig. 10a), the columnar stromatolite *Murmania sidorenkia f. Nova Ljubtsov* was reported from one locality situated 30 km south-east of the drilling site (Lybtsov 1979). Layering of the microbial dolostones is expressed by alternation of silty to sandy allochemical dolostone and algal micritic dolostone. The latter exhibits a microstructure expressed by alternation of 0·2–1·0-mm-thick dolomicrite laminae and 0·1–0·3-mm-thick laminae consisting of finely crystalline quartz and sparry dolomite. Variably developed fenestrae (Fig. 10b, c), and intensive syn-sedimentary brecciation and buckling (Fig. 10b–d) are common. In places, the flat-laminated stromatolites are discordantly capped by a travertine crust (Fig. 9b).

The sandy, micritic, allochemical dolostones comprise irregularly distributed, 5- to 10-cm-thick layers, although a 2-m-thick bed occurs in the uppermost part of the unit (Fig. 4). Allochems are both angular, platy and rounded clasts of massive micritic dolostone, and algal micritic dolostone. The carbonate clasts which are larger than 0·5 cm have a platy form, whereas the smaller clasts are usually spherical. In some cases, the sandy, allochemical dolostones grade into dolomite-cemented quartzitic sandstones (Fig. 9c). Fenestrae may be very abundant in some layers, particularly in those containing plentiful clasts of algal dolostones. Brecciation and deformation related to tepees have been observed in both drillcores and outcrops. The allochemical and micritic dolostones contain small crystals of authigenic albite and 1–4-mm spherical inclusions of sparry dolomite.

5.4.3. Siliciclastic-dominated Unit VIII. Unit VIII occurs in the middle of the Dolostone Member and is 2·2 m thick (Figs 2 & 4, Table 2). It consists of carbonate breccia (Fig. 9d) interbedded with sericite-chlorite mudstones, followed by quartz sandstone. The breccia is red, clast-supported and consists of highly disrupted dolostone beds overlain by angular, unsorted and closely packed fragments of red and pink dolostone in a chlorite matrix (Fig. 9d). The mudstone is marked by planar lamination and contains a series of small-scale (3 × 0·5 mm), siltstone-filled, erosional scours. Clasts of quartz and microcline are angular, for the first time in the entire formation (Table 4). This also marks the first appearance of substantial amounts of chlorite and accessory pyrite (Table 4). Unit VIII ends with 1·2-m-thick coarse-grained sandstone.

5.4.4. Dolostone-dominated Unit IX. Unit IX is a 9-m-thick unit consisting of homogeneous, sandy, sparry, allochemical dolostones with crude cross-lamination. In places, bedding planes are marked by scouring (Fig. 9e).

5.4.5. Dolostone-dominated Unit X. Unit X is 9·2 m thick (Fig. 4, Table 2) and consists of four types of interbedded rocks: (1) microbial; (2) sandy, sparry allochemical; (3) micritic dolostone; and (4) abundant travertine crusts and small-scale travertine mounds (Table 2). All lithologies have either a pink or variegated colour with a mottled appearance (Fig. 11). The microbial dolostones display flat-laminated varieties (Figs. 11a, b), although some of them exhibit undulatory or weakly-domed structures (Fig. 11a). They are commonly composed of 1- to 2 cm-thick layers of microbial laminites interbedded with 1- to 3-cm-thick layers of pink and brown, dolomicrite. The microbial layers consist of 0·2- to 0·5-mm-thick, irregular laminae of micritic dolomite (primarily microbial mats), thicker layers of sparry dolomite containing carbonate intraclasts and quartz detritus, and chert-filled fenestrae (Fig. 11c). In many cases, the microbial lamination is highly disrupted by desiccation features and formation of micronodules of probable evaporites pseudomorphed by chert and dolomite. Consequently, microbial dolostones display microbrecciation and are the source of clasts in the interbedded allochemical dolostones. The stromatolitic dolostones also contain tepee structures (Fig. 11d, e). Beds located above the tepees are affected by development of pedogenic dolocrete and silcrete (Fig. 11d; Melezhik *et al.* 2004) and contain abundant silica sinters (Fig. 11e). Tepee-related cracks and voids have also been found filled with sparry dolomite and talc.

The sandy, sparry, allochemical dolostones are pink or mottled, and contain both rounded and platy unsorted intraclasts of micritic and algal dolostones (Fig. 11f). The allochemical dolostones contain abundant dissolution microcavities of a subaerial origin (Melezhik *et al.* 2004). The

https://doi.org/10.1017/S0263593300001140 Published online by Cambridge University Press

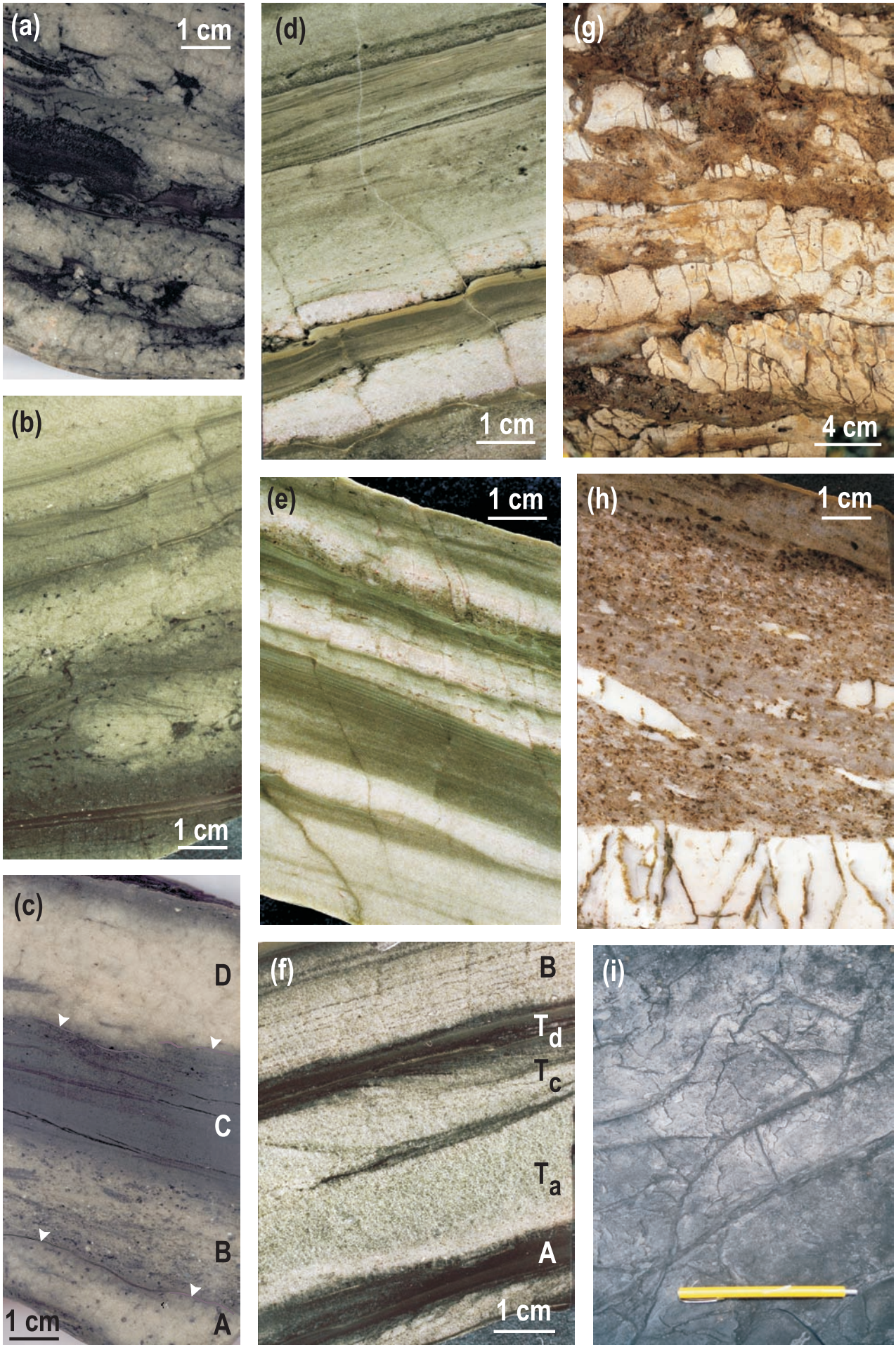

https://doi.org/10.1017/S0263593300001140 Published online by Cambridge University Press

microcavities are usually veneered by silica sinter and marked by reddening (Fig. 11f). The cavities are commonly filled with sandy allochemical dolostones.

The micritic dolomites form 2- to 10-cm-thick beds interlaminated with allochemical and algal dolostones. They contain dolomite-pseudomorphed micronodules of probable evaporites (Fig. 11g). All dolostone lithologies are associated with abundant travertine crusts and small-scale travertine mounds (Fig. 11h), as described in detail by Melezhik & Fallick (2001).

5.4.6. Mixed siliciclastic-dolostone Unit XI. Unit XI is only 0·2 m thick (Fig. 4) and marks the last sedimentary deposit prior to the subaerial volcanic eruptions which resulted in the formation of 2000-m-thick volcanic rocks. The unit consists of chlorite-cemented sandstones (Table 2), and in the areas adjacent to the drilling site, chlorite-cemented, intraformational dolostone breccias.

5.5. Palaeoenvironmental interpretation of Dolostone Member, Units VI-XI

The Dolostone Member consists of six units. The lowermost unit, VI, contains thin films of the flat-laminated microbial mats and encrustations, which are both of palaeoenvironmental significance. Flat-laminated, globular and granulated microbial mats are common features of some modern lakes and isolated shallow-water lagoons (e.g. von der Borch 1976; Srivastava & Almeida 2000). In deep lakes, like Lake Tanganyika, microbial encrustations occur at very shallow depths (i.e. 1·5–14 m; Cohen *et al*. 1997). In the marine environment, low-relief, flat-laminated stromatolite sheets are usually accreted in zones where wave and tidal scour was weak, such as coastal sabkhas, drained depressions and ephemeral ponds in a supratidal or upper tidal zones of a carbonate flat (e.g. Kinsman & Park 1976). Proterozoic laminated tufa and microbial laminates have commonly been accumulated on an intertidal to supratidal, low-energy tidal flat (Southgate 1986; Grotzinger 1989; Kah & Knoll 1996). Based on these criteria, the Unit VI dolostones containing thin films of stromatolites and encrustations are considered to represent a shallow-water to shoreline low-energy setting.

Unit VII contains abundant travertine crusts, flat-laminated microbial sheets and tepees, which are all indicative of a coastal carbonate plain. Abundant travertine deposits and silica sinters (Melezhik & Fallick 2001) are typical features of many hot-spring-influenced terrestrial depositional settings (Jones & Renaut 1997; Jones *et al*. 1997, 1998) and lacustrine sediments in modern continental rift environments (Renaut *et al*. 1986, 1998; Renaut & Tiercelin 1994; Renaut & Owen 1998). The hydrothermal deposits of Unit VII suggest that the carbonate depositional system was episodically influenced by hydrothermal springs. Inclusions of authigenic albite and 1–4-mm spherical inclusions of sparry dolomite (Fig. 11g) resemble micron-scale euhedral pseudomorphs after calcium sulphates reported from late Triassic rift basin lacustrine sediments (El-Tabakh *et al*. 1997). The presence of authigenic albite and dolomite-pseudomorphs of probable sulphate micronodules may indicate an arid climate and evaporitic conditions (e.g. Behr *et al*. 1983). The significant disruption of microbial sheets is considered to be the result of dewatering and desiccation of cyanobacterial mats. This, in turn, indicates a frequently drying out, shallow-water depositional system. The tepee structures documented throughout the sequence (Table 2, Fig. 4) support this inference. Evaporative pumping is usually most effective in an arid climate along a coastal plain (e.g. Demicco & Hardie 1994).

Unit VIII chlorite-cemented dolostone breccia (Table 2, Fig. 9b) indicates reworking of carbonate sediments previously formed on the carbonate flat with subsequent local transport of carbonate clasts and their incorporation into the siltstones. The presence of thinly laminated siliciclastic material with microscopic-scale, mud-filled channels suggests that the basin experienced an episode of sediment starvation. Abundant chlorite is indicative of possible influence of a mafic volcanism, which could also be considered as a source of the sulphur. The volcanic event is considered to have been linked to rift propagation.

The sedimentological information available for Unit IX (Fig. 4, Table 2) does not provide enough criteria for the reconstruction of depositional environments. The presence of small-scale channels, and the abundance of rounded intraclasts of micritic dolostones suggests reworking of the carbonate-dominated coastal plain and shoreline.

The environmental constraints of Unit X are provided by abundant travertine crusts and silica sinters (Melezhik & Fallick 2001), flat-laminated desiccated microbial sheets, subaerial silcretes and dolocretes (Melezhik *et al*. 2004), and 'red beds' (Table 2). Similarly to Unit VII, these facies imply a non-marine environment because travertine mounds and tufa have mostly been reported from coastal marshes, lake shores, springs, rivers and waterfalls (Renaut *et al*. 1986; Demicco & Hardie 1994). Surface silicification (silcrete) of carbonate rocks has been commonly found from continental limestones and dolostones, including lacustrine types (Freytet 1973). Hydrothermal surface silicification and silica sinters are widespread phenomena of hydrothermal areas (Jones *et al*. 1996, 1997, 1998; Jones & Renaut 1997) and are particular characteristics of many modern lacustrine depositional settings in continental rift environments (Renaut *et al*. 1986, 1998; Renaut & Owen 1988; Renaut & Tiercelin 1994; Behr 2002). The red colour developed throughout Unit X suggests that the depositional

Figure 6 Core and outcrop photographs of Unit II. Core photos denoted as drill hole X (DHX) with depth-in-core given in metres. (a) Soft-sediment loading and small-scale incipient 'ball-and-pillow' structures along bases of light-coloured sandstone beds into dark-coloured mudstone layers (DHX 391·0); (b) Thin, graded sandstone-to-mudstone (basal mudstone is haematite rich) beds displaying flat- to wavy-parallel lamination and unidirectional ripple cross-lamination. Note the loading and small-scale scouring along the base of the sandstones (DHX 390·6); (c) Apparently structureless sandstone (A) overlain erosionally by sandstone bed (B) with mud rip-up intraclasts. This bed passes abruptly upward into purple siltstone (C), marked by flat- to unidirectionally migrating low-angle lamination, which is, in turn, erosionally overlain by a light-coloured sandstone bed (D). Note the purple siltstone intraclasts in its basal part. White arrows denote erosional scour surfaces (DHX 389·7); (d) Sharp-based graded sandstone beds. Beds display variably developed Bouma sequences, from massive bases to faintly parallel laminated sandstone to ripple cross-laminated and wavy- to low-angle laminated mudstone (dark coloured layers). Note that ripple cross-laminae show unidirectional migration directions and that some of the mudstones display loading structures (DHX 386·5); (e) Thinly interbedded fine sandstone (light coloured) and siltstone (dark coloured) exhibiting planar to low-angle ripple cross-lamination. Grading can be seen in the upper two sandstone beds (DHX 382·7); (f) The Bouma sequence (above lower dark siltstone layer, A) exhibit uneven spacing and are composed of a light-coloured, graded-bedded and massive sandstone (T_a, 3 cm thick), a unit of light-coloured, cross-bedded silty sandstone (T_c, 1·5 cm thick), and a thin, planar-laminated, dark-coloured mudstone (T_d, 1 cm thick), followed by the next graded-bedded, light-coloured sandstone layer (B). The lowermost sandy layer has been cleaved with a cleavage direction opposite to that of the ripple cross-lamination (DHX 385·9); (g) Sedimentary breccia consisting of dolomicrite clasts (light yellow) encased in a muddy sandstone matrix. The exposure is 7 km west of DHX (Fig. 1); (h) Imbricated intraclastic sedimentary breccia comprised of dispersed, tabular, dolomicrite clasts in a muddy sandstone matrix. The breccia bed sits sharply on underlying dolomicrite (DHX 381·6); (i) Probable desiccation cracks in mudstone. The exposure is 7 km west of DHX (Fig. 1). The pencil is 15 cm long.

https://doi.org/10.1017/S0263593300001140 Published online by Cambridge University Press

settings, in which the 'red beds' were accumulated, were frequently emerged and exposed to oxygen-rich air, thus representing a non-marine, terrestrial environment. The abundant hot-water travertine deposits (Melezhik & Fallick 2001) are evidence of active surface hydrothermal activity (Renaut *et al*. 1986; Chafetz *et al*. 1991; Guo & Riding 1992; Jones & Renaut 1996; Renaut & Jones 1997). Constraints on climatic conditions are provided by the highly disrupted lamination caused by desiccation cracks, and formation of chert- and dolomite-pseudomorphed micronodules of probable evaporites. All these features are consistent with a semi-arid climate. This is also supported by widely developed tepee structures.

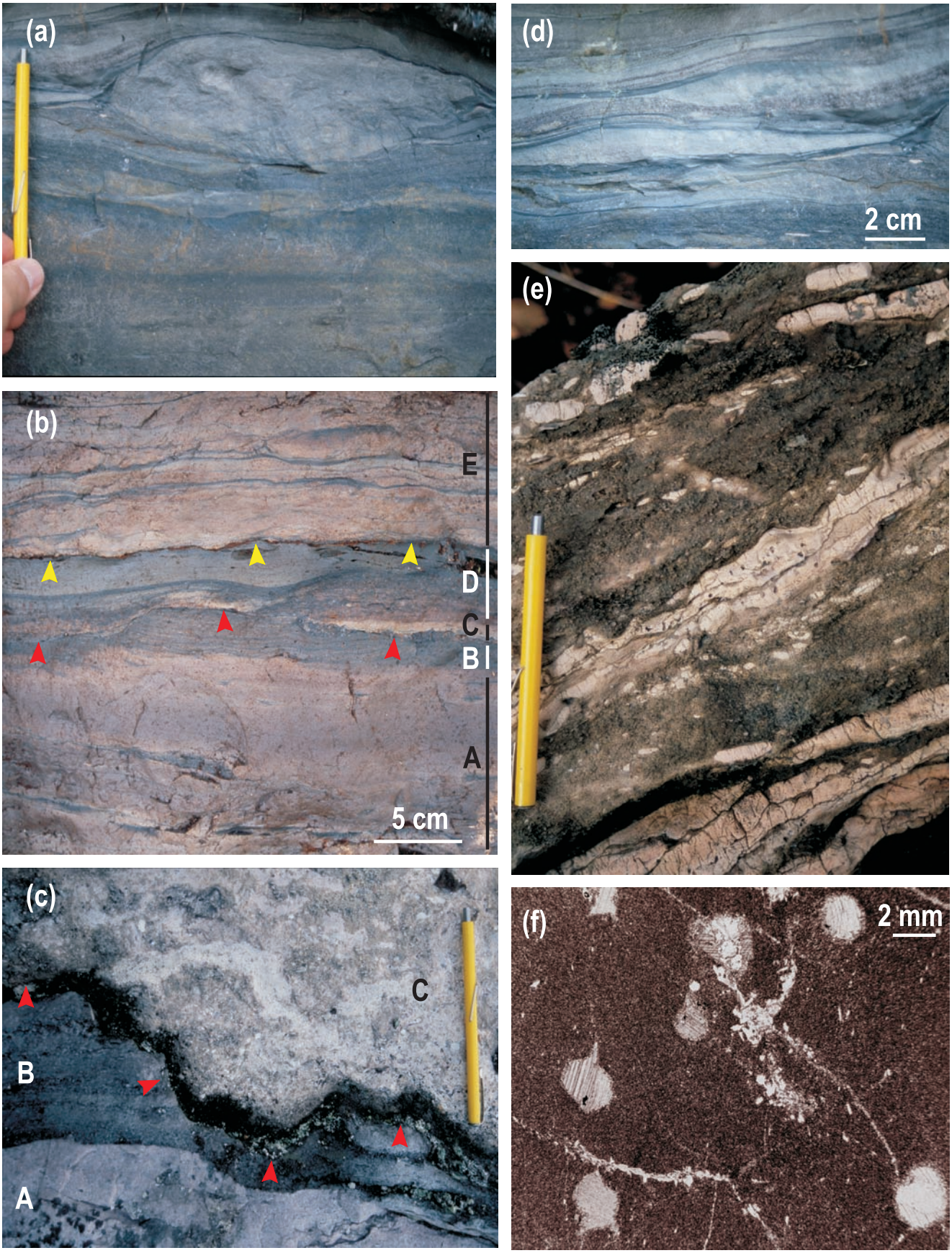

https://doi.org/10.1017/S0263593300001140 Published online by Cambridge University Press

The surface micro-cavities and dolocretes veneered with silcrete (Melezhik *et al*. 2004) are of particular significance since they are indicators of subaerial exposure without detrital sedimentation for a significant period of time (Demicco & Hardie 1994; Alonso-Zarza 2003). Although tepee-related brecciation and evaporite precipitation occurred most frequently under relatively arid conditions, the synsedimentary deformation and displacive mineral growth has been reported from hydrothermal spring deposits (e.g. Renaut *et al*. 2002).

Unit XI chlorite-cemented, intraformational, dolostone breccias are likely an unconformity breccia developed subaerially as a result of reactivation of the rift prior to a new phase of volcanic eruption and deposition of 2000-m-thick volcanic rocks overlying the KSF. Considerable enrichment of all rocks in chlorite indicates the initiation of basaltic volcanism. In summary, the Dolostone Member contains evidence for deposition under overall arid climate in lacustrine and shoreline settings.

6. Main geochemical features of siliciclastic and carbonate rocks

6.1. Siliciclastic rocks

Geochemically, siliciclastic rocks approximate to three major groups: a quartzitic sandstone, arkosic sandstone, and sericitic siltstone and mudstone (Table 5, Fig. 12). All rocks are markedly enriched in K_2O, by up to 11 wt.%, and characterised by a low concentration of Na_2O. This perhaps indicates that potassium-rich granites dominated in the provenance area. The arkosic sandstones dominate over silica-rich varieties and sandstones containing >85 wt.% SiO_2 have been found only in units II and VIII (Fig. 12). The sandstones are texturally rather mature (Table 4), suggesting that the area adjacent to the depositional site was characterised by low-relief, allowing a high degree of mechanical sorting of clastic components. In contrast, the chemical maturity, as indicated by a low degree of alteration of the feldspar clasts, and high K_2O concentration in the rocks (Table 5), is moderate. This indicates an arid to semiarid climate.

Almost all the rocks contain dolomite and calcite, which appear as cement, and cause elevated CaO and MgO concentrations. The red siltstones and mudstones of units V and VI are relatively enriched in Fe_2O_3. All rocks are very low in S_{tot}, although some Unit VIII rocks may contain up to 0·5 wt.% S_{tot}, and the concentration of C_{org} is below the detection limit of 0·1 wt.%. The very low S_{tot} and C_{org} concentration, and abundant 'red beds' are consistent with a non-marine, freshwater, oxygenated environment resulting in rapid oxidation of biologically produced sulphides and organic matter. The low S_{tot} concentration might have also been caused by a limitation of sulphate in the depositional system. This might have suppressed biological reduction of sulphates and prevented formation of sulphides, all suggesting a non-marine, sulphate-poor basin.

The mottled siltstones of Unit IV exhibit a relative accumulation of P_2O_5. These rocks are also marked by the development of authigenic apatite whereas other lithofacies contain clastic apatite (Table 4). Enrichment in P_2O_5 is considered to be a post-depositional phenomenon genetically associated with bleaching and discoloration of the 'red beds' which was caused by introduction of H_2S-free and P_2O_5-rich, reducing fluids (Melezhik 1992).

6.2. Carbonate rocks

The MgO and CaO concentrations indicate that most of the carbonate rocks approximate to a dolostone (Table 6, Fig. 13). The carbonate breccia from Unit VIII (296·54 m) possibly contains minor magnesite, as indicated by an elevated MgO/CaO ratio (Fig. 13). Limestones are uncommon, occurring either as interbeds in siliciclastic sediments or thin layers within dolostone lithofacies. In the latter case, the limestone is commonly developed in contacts between siliciclastic and dolostone-dominated lithofacies. Replacement textures suggest that the limestones are the result of dedolomitisation. High overall SiO_2 values indicate that the major siliciclastic component is quartz. Like the siliciclastic lithofacies, the dolostones are enriched in K_2O with respect to Na_2O. The latter is often below 0·01 wt.% and the C_{org} concentration is always below the detection limit of 0·1 wt.%. Two thin intervals of dolostones enriched in P_2O_5 and S_{tot} occur in units VII and VIII (Fig. 13); otherwise, dolostones exhibit rather low concentrations of these compounds. An elevated concentration of P_2O_5 with concomitant enrichment in S_{tot} is considered to have been generated by biological activity. This may include (1) an accumulation of biologically produced C_{org} and P_2O_5, with (2) subsequent degradation of C_{org} and bacteriogenic reduction of sulphate, and (3) the formation of sulphides.

7. Basinal evolution

The available geological data suggest that the depositional site was a rift-related basin lake which was formed by tectonic processes on a rifted continental margin of an Archaean plate. The rift formation was preceded by a prolonged non-depositional break (duration not known) and the formation of regolith (Sturt *et al*. 1994). The rift-forming tectonic processes produced half-graben structures (Melezhik & Sturt 1994) filled with fluviatile deposits and subaerially erupted volcanites which were affected by intensive subaerial weathering. A further phase of gentle, low-amplitude subsidence formed a shallow-relief basin in which the Kuetsjärvi lake developed.

The KSF bears many characteristics of modern and ancient lake sediments of which the following are salient: (1) it lies on a palaeoweathered crust; (2) the sedimentary sequence is sealed between two, 2-km-thick volcanic formations which were each

Figure 7 Outcrop and thin-section photographs of Unit II. The thin-section photograph is from the core denoted as drill hole X (DHX) with depth-in-core given in metres. (a) Slumped horizon in an interbedded fine sandstone–siltstone interval. Note how the slump appears to be draped and possibly onlapped by (lefthand side of the slump) overlying layers. The exposure is 7 km west of DHX (Fig. 1). The pencil is 15 cm long. (b) The lower part of the photograph shows a pale brown siltstone bed (A) containing finer intraclast (darker coloured) that grades upward into wavy- to flat-parallel mudstone (B) that is sharply truncated and eroded (erosion surface marked by red arrows) by thin-based sandstone bed (C) that passes rapidly upward into wavy-laminated mudstone (D). This bed is overlain erosionally (small-scale basal scour marked by yellow arrows) by another thin sandstone that grades upward into wavy-parallel laminated and wispy-bedded siltstone-mudstone (E). The exposure is 7·5 km west of DHX (Fig. 1); (c) Small channel (marked by red arrows) filled with poorly sorted dolarenite (C). The channel cuts into an underlying bed of dark purple, haematite-rich, arkosic siltstone (B) and pale purple arkosic sandstone (A). The exposure is 8·2 km west of DHX (Fig. 1). The pencil is 15 cm long; (d) Lenticular, wavy and linsen-bedded (starved ripples) fine sandstone and siltstone. The exposure is 8 km west of DHX (Fig. 1); (e) Thin, irregular, undulose-bedded dolostones alternated with very poorly sorted, matrix-supported, intraclastic (clasts are dolomicrites) sedimentary breccias. The exposure is 8·6 km west of DHX (Fig. 1). The pencil is 15 cm long; (f) Photomicrograph in transmitted non-polarised light of dolomicrite showing spheroidal and castellated margin inclusions filled with sparry dolomite (DHX 382·6).

https://doi.org/10.1017/S0263593300001140 Published online by Cambridge University Press

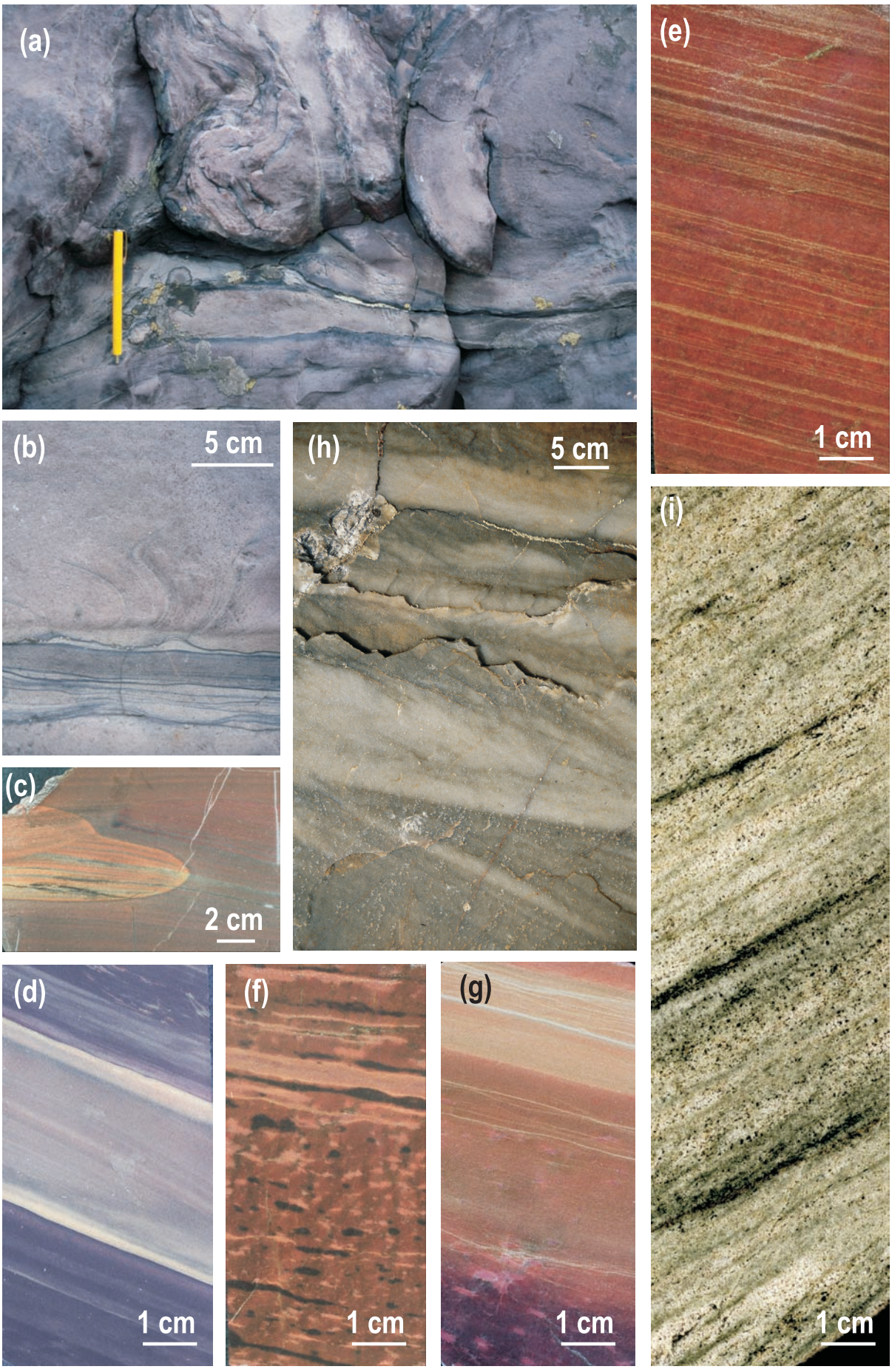

https://doi.org/10.1017/S0263593300001140 Published online by Cambridge University Press

Table 4 Characteristics of clastic material from clastic-dominated units of the Kuetsjärvi Sedimentary Formation (drill hole X)*

Unit	Clast composition	Rounded (unrounded)	Sorted (unsorted)	Weathered (unweathered) Ksp and Pl	Clast size (mm)	Accessory mineral	Authigenic mineral	Matrix
Unit VIII:								
Siltstone	Qz, Ksp	(–)	(–)	(–)	0·03–0·06	Tour	Py	Ser, Dol, Chl
Sandstone	Qz	+	(–)	(–)	0·4–1·0	–	Py	Qz, Dol
Unit V:								
Sandstone	Qz, Ksp, Ms	+	(–)	(–)	0·04–1·2	Tour, Zr	Tour, Ap	Ser, Dol
Unit IV:								
Upper part, siltstone	Qz, Ksp, Pl, Ms, Ha	+	+	(–)	0·02–0·08	Tour	Ap	Ser, Dol
Lower part, mudstone	Qz, Ksp, Ha	+	+	(–)	<0·001–0·01	–	Tour	Ser
Unit III:								
Sandstone, siltstone	Qz, Ksp, Pl, Ha	+	(–)	(–)	0·02–0·4	–	Ap	Qz, Ser
Unit II:								
Upper part, sandstone	Qz, Ksp, Ms, Bt	+	(–)	(–)	0·3–1·0	Tour	Dol	Qz, Ser, Dol
Middle part, sandstone	Qz, Ksp, Bt	+	(–)	(–)	0·07–0·8	Tour	Dol	Qz, Ser, Dol
Lower part, sandstone	Qz, Ksp, Pl, Bt	+	(–)	(–)	0·05–0·1	Tour	Dol	Qz, Ser, Dol

*Abbreviations: (Ap) apatite; (Bt) biotite; (Chl) chlorite; (Dol) dolomite; (Ksp) microcline; (Ha) haematite; (Ms) muscovite; (Pl) plagioclase; (Py) pyrite; (Qz) quartz; (Ser) sericite; (Tour) tourmaline; and (Zr) zircon.

subaerially erupted; (3) it is of modest thickness; (4) it exhibits rapid vertical variation of sedimentary facies; (5) it contains abundant travertine deposits; (6) clastic sediments are fine-grained; (7) high impurity of carbonate rocks; (8) flat-laminated microbial sheets; (9) low concentration of sulphides; (10) abundant 'red beds', variegated and mottled rocks; and (11) surface silicification. Taken together, and given the dearth of evidence for tides (neither flaser and lenticular bedding, bidirectional cross-bedding, nor rhythmites with mud drapes have not been found), the inference that the KSF formed in a non-marine environment is supported strongly.

7.1. Early stage

The history of the rift-related lake can be divided into three phases. The first or juvenile stage includes rifting and formation of an elongated, low-relief half-graben which were complicated by a series of transverse faults and small-scale transverse grabens (Fig. 14). The conservative estimate suggests that the lake could attain ca. 100 km in length, although the width remains unknown. This stage is marked by accumulation of braidplain and braid-delta sediments fringing the lacustrine basin. The fill of the Kuetsjärvi basin tends to be predominantly red and purple in colour, fine-grained and finely laminated, suggesting that the lake was rather shallow. All clastic material was transported from long distances, as indicated by the high degree of clast roundness and by the lack of clasts derived from the underlying andesitic basalts. Red, haematite-rich laminites indicate a highly oxygenated waterbody. A limited amount of carbonate material, which was precipitated during this stage, was related to mixed dolostone–siliciclastic facies. Carbonates were apparently precipitated in several ways and mainly in interdistributary areas along the shoreline. Non-marine carbonate accumulation may be achieved by deposition from clastic load, springs, groundwater discharge, soil and karst development, biochemical seasonal changes, and eolian influx (Evans & Welzenbach 1998; Gierlowski-Kordesh 1998 and references therein). The clastic load should not be considered because carbonate-rich source provenances are absent in areas adjacent to the Pechenga palaeorift (Melezhik *et al.* 1995). The eolian influx is not consistent with the sporadic appearance of massive dolostone lenses interbedded with sandstones and siltstones (Figs 6g, 7e). The springs, groundwater discharge and biochemical seasonal changes cannot be ruled out. The most important factor controlling the inorganic precipitation of carbonates at this stage was carbonate supersaturation, which was probably caused by the evaporitic degassing of CO_2. Formation of pedogenic carbonates (Melezhik *et al.* 2004) and biologically induced precipitation was likely of secondary importance.

7.2. Middle stage

The second phase of lake development is marked by accumulation of carbonate precipitates, mainly dolomite. Dolomite was precipitated and became a major component of the lake infill where supplies of clastic material were suppressed (Fig. 14). The sedimentological data suggest that the carbonate lithofacies were accumulated in shallow water adjacent to and/or along a carbonate shoreline setting, and subject to frequent variation of water level. The lake margins must have had a low relief gradient, resulting in the extensive development of exposed areas during low-water periods. The water level and composition apparently depended on three factors:

Figure 8 Core and outcrop photographs of Units III–V. Core photographs denoted as drill hole X (DHX) with depth-in-core given in metres. (a) Unit III: 'Ball-and-pillow' structure in arkosic sandstones. Sandstone beds are separated by thin, haematite-rich mudstone beds (note the upward injection of mudstone into and between the 'ball-and-pillow' structure). The exposure is 8 km west of DHX (Fig. 1). The pencil is 15 cm long; (b) Unit III: Injection (air heave or fluid escape?) structure in an otherwise massive sandstone bed overlying thinly interbedded siltstones and fine sandstones separated by filamentous wisps to more continuous partings of mudstone. The exposure is 8 km west of DHX (Fig. 1); (c) Unit III: Small-scale, trough cross-bedded, fine sandstone. The brighter-coloured region ('roll') is caused by migration of reducing fluids during catagenesis. The sample was collected 20 km southeast of DHX; (d) Unit IV: Finely laminated, haematite-rich, mudstone–siltstone interbeds. The lighter-coloured layer was caused by infiltration of catagenetic reducing fluids (DHX 356·7); (e) Unit IV: Haematite-rich siltstone with fine, varve-like lamination (DHX 356·4); (f) Unit IV: 'Mottled' siltstone. The darker-coloured layers are primary sedimentary laminae whereas the lighter-coloured layers and blebs are caused by reduction by migrating catagenetic fluids (DHX 355·2); (g) Unit IV: Finely laminated variegated siltstone. Lighter colours are caused by migration of catagenetic fluids (DHX 353·5); (h) Unit V: Stacked cross-bed co-sets in quartzitic sandstone. The exposure is 7·8 km west of DHX (Fig. 1); (i) Unit V: Stacked cross-bed co-sets (possibly climbing ripples?) in dolomite-cemented arkosic sandstone (DHX 345·7).

https://doi.org/10.1017/S0263593300001140 Published online by Cambridge University Press

(1) overall slow tectonic subsidence; (2) a water inflow controlled by precipitation, run-off during rainy periods and hydrothermal springs, and (3) any possible connections with sea. Given the data presented here, the latter seems unlikely, but remains to be falsified. The periods of extremely low water levels, when playa-like conditions existed (as evident from tepees, desiccated microbial sheets and traces of probable dolomite-pseudomorphed sulphates), led to the deposition of the main volume of carbonates (Units VII and X). Fluctuations in lake level led to phases of emergence and submergence, and during the former, silcretes and dissolution surfaces were developed. Abundant carbonate travertine deposits were associated with surface pools fed by hot-water springs (Melezhik & Fallick 2001). Dolomite precipitation was apparently biologically meditated and promoted by arid to semi-arid climatic conditions, as suggested by abundant flat-laminated microbial

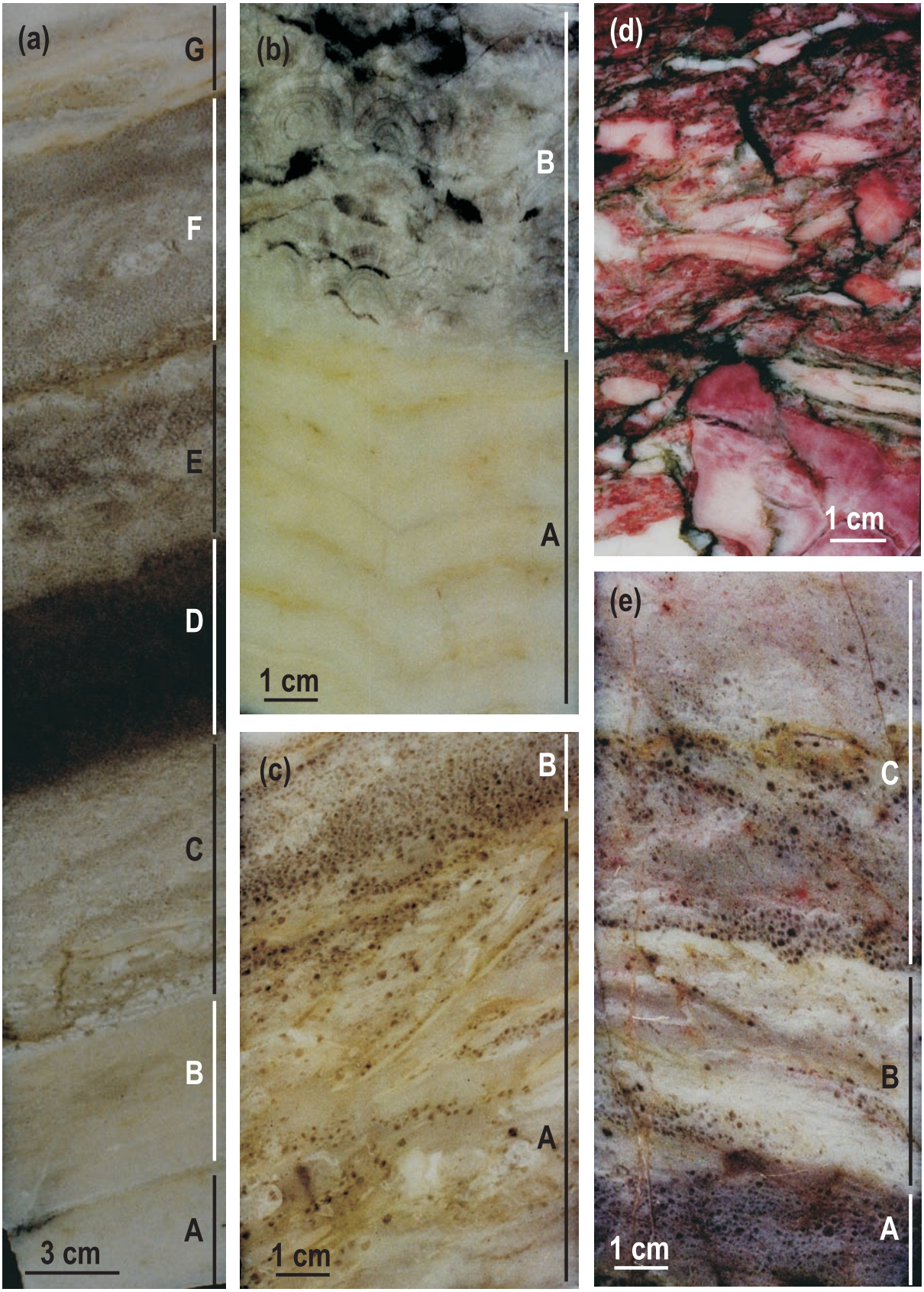

https://doi.org/10.1017/S0263593300001140 Published online by Cambridge University Press

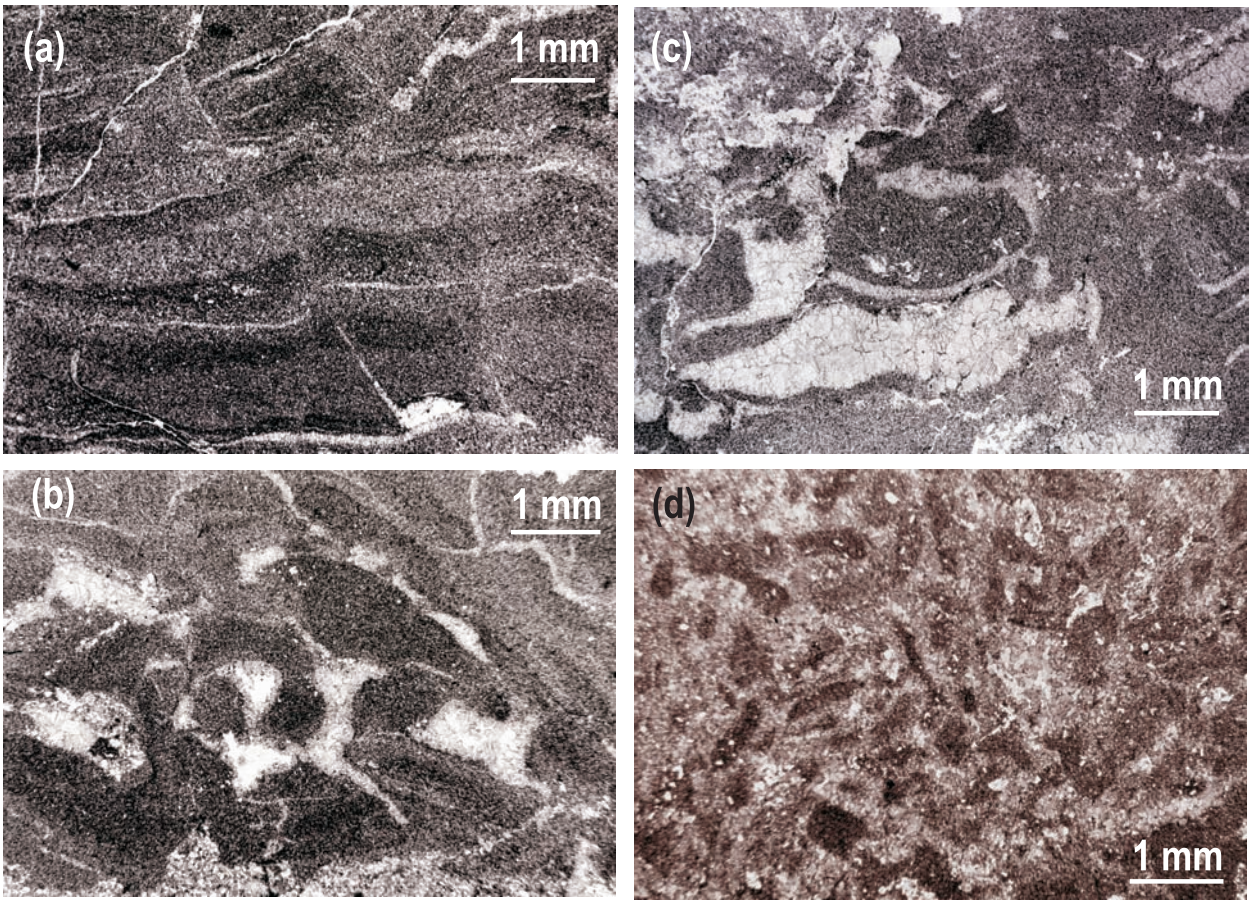

Figure 10 Transmitted plane-polarised light photomicrographs of Unit VII dolostones from core drill hole X (DHX) with depth-in-core given in metres. (a) Finely laminated, stromatolitic dolomicrite. Darker and thinner laminae represent the microbial mat, whereas lighter and thicker laminae consist of fine quartz sand and microsparite (DHX 308·8); (b) Brecciated microbial dolostone with abundant fenestrae filled with sparry dolomite (DHX 308·9); (c) Brecciated and buckled microbial dolomicrite containing dolospar-filled desiccation cracks and fenestrae. Fragmentation and intraclast development were caused by desiccation (DHX 306·9); (d) Intensively brecciated microbial dolomicrite (DHX 298·4).

mats which were frequently exposed, intensively brecciated, disrupted by crystal growth and silicified.

Significant accumulation of carbonate rocks is not unusual in modern and ancient lacustrine settings, and carbonate sediments may constitute an essential part of lake infill. This has been reported from the Green River Formation, Utah, USA (Picard & High 1981), the Las Minas Basin, Spain (Calvo *et al.* 2000), Lake Constance, Germany (Schottle & Müller 1968), and the Caspian Sea, Russia (Klenova 1968). Carbonate precipitation may be rapid. Summer 'whitings' (seasonal clouding of the epilimnion by $CaCO_3$) have been observed in many closed lakes (Brunskill 1969; Strong & Eadie 1978). Furthermore, most well-studied ancient lacustrine carbonates indicate that shallow-water conditions and ancient playa-lake sediments may attain considerable thicknesses of 1000 m and more (Talbot & Allen 1996).

Carbonate sediments in lacustrine environments are commonly formed by several processes discussed in detail by Talbot & Allen (1996). Sedimentological data indicate that the most important single factor controlling the precipitation of the Kuetsjärvi carbonates was apparently carbonate saturation caused by microbial photosynthesis and evaporitic degassing of CO_2. The rate of both inorganic precipitation and bio-induced precipitation of carbonate minerals was enhanced by shallow-water conditions and the development of a playa surface (Fig. 14). Hot-spring waters are considered to have

Figure 9 Core and outcrop photographs of Units VI–IX. Core photographs denoted as drill hole X (DHX) with depth-in-core given in metres. (a) Unit VI: Core showing the following facies. The lowermost layers (A and B) are massive dolomicrite sharply overlain by cross-laminated allochemical (dolomicrite intraclasts) dolostone (C) with clotted structure that grades into dark-coloured, dolomite-cemented quartzitic sandstone (D); in turn, this is overlain by two other allochemical dolostone layers (E and F) which are sharply capped by light-coloured, faintly laminated dolomicrite (G). Note the small erosional scours along base of allochemical dolostone layers (DHX 337·4); (b) Unit VII: Light-coloured, faintly microbially laminated, micritic dolostone (A) sharply capped by darker travertine crust (B). The dolostone consists of indistinctly undulatory and almost rhythmical lamination defined by couplets of thinner, yellowish dolomicrite and thicker white microdolospar. The crust is composed of clusters of small-scale, semi-spheroidal travertine mounds exhibiting radial fabrics and irregularly developed siliceous sinters (dark-coloured) (DHX 310·2); (c) Unit VII: Allochemical sandy dolostone (A) overlain by quartzitic sandstone with dolomite matrix (B). The buckled platy intraclasts are probably related to development of tepee structures. The sandy material consists of well-rounded and sorted quartz grains (DHX 314·8); (d) Unit VIII: Clast-supported dolorudite. Clasts are variegated dolomicrite in a dark mudstone matrix (DHX 297·7); (e) Unit IX: Indistinctly cross-bedded sandy dolostone. Note the syn-sedimentary folding near top of middle layer (B), which is sharply and erosively overlain (small scour along base of bed) by the upper sandy dolostone bed (C) (DHX 283·7).

https://doi.org/10.1017/S0263593300001140 Published online by Cambridge University Press

played an important role in carbonate precipitation in the Kuetsjärvi lake. The importance of hot springs in lacustrine sedimentation has been acknowledged in many Recent lakes from the East African Rifts (e.g. Renaut & Tiercelin 1994).

7.3. Late stage

The third and terminal stage of the Kuetsjärvi basin was manifested by an abrupt subsidence (renewed rift) followed by voluminous volcanism. This stage is recorded in Unit XI

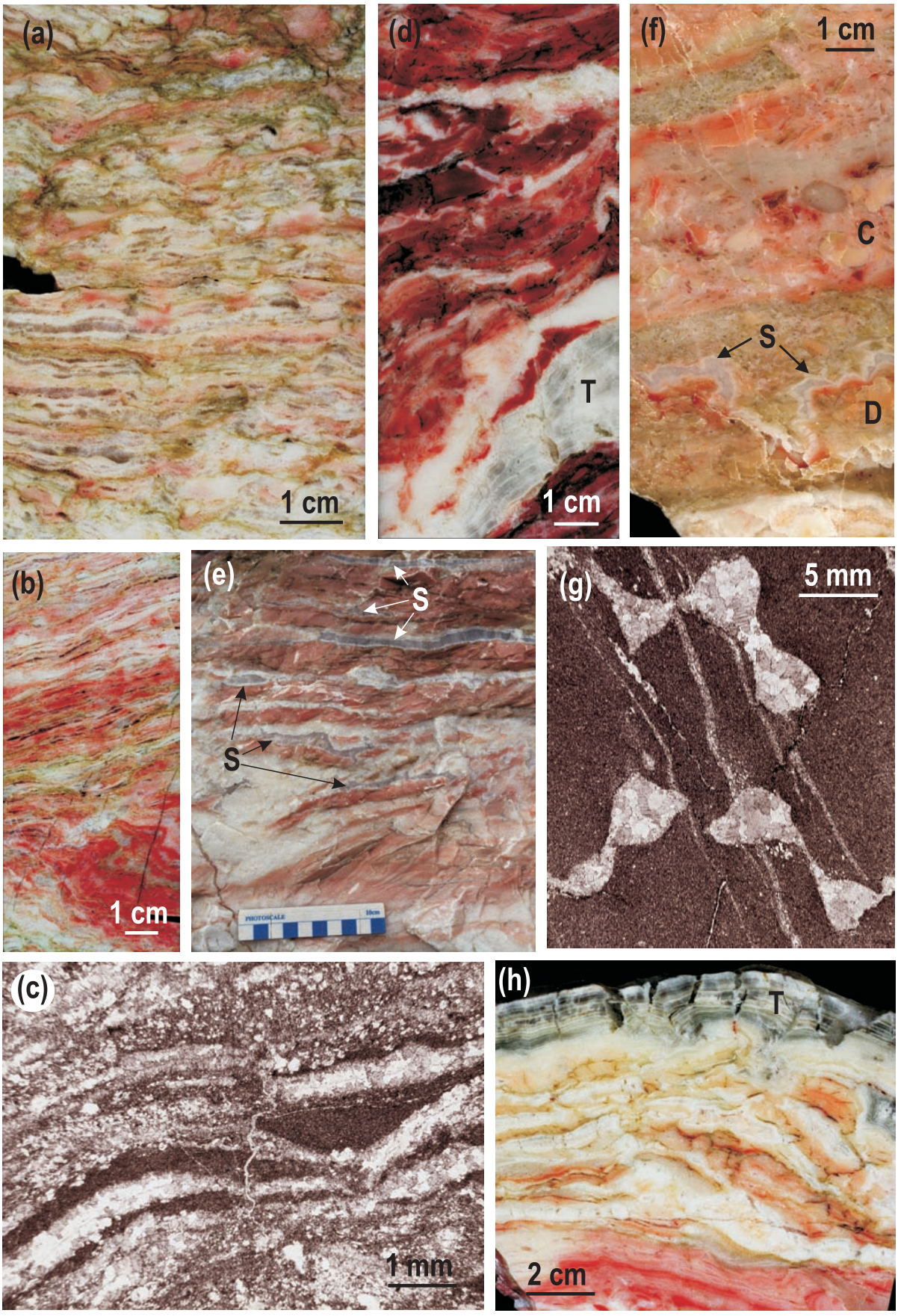

https://doi.org/10.1017/S0263593300001140 Published online by Cambridge University Press

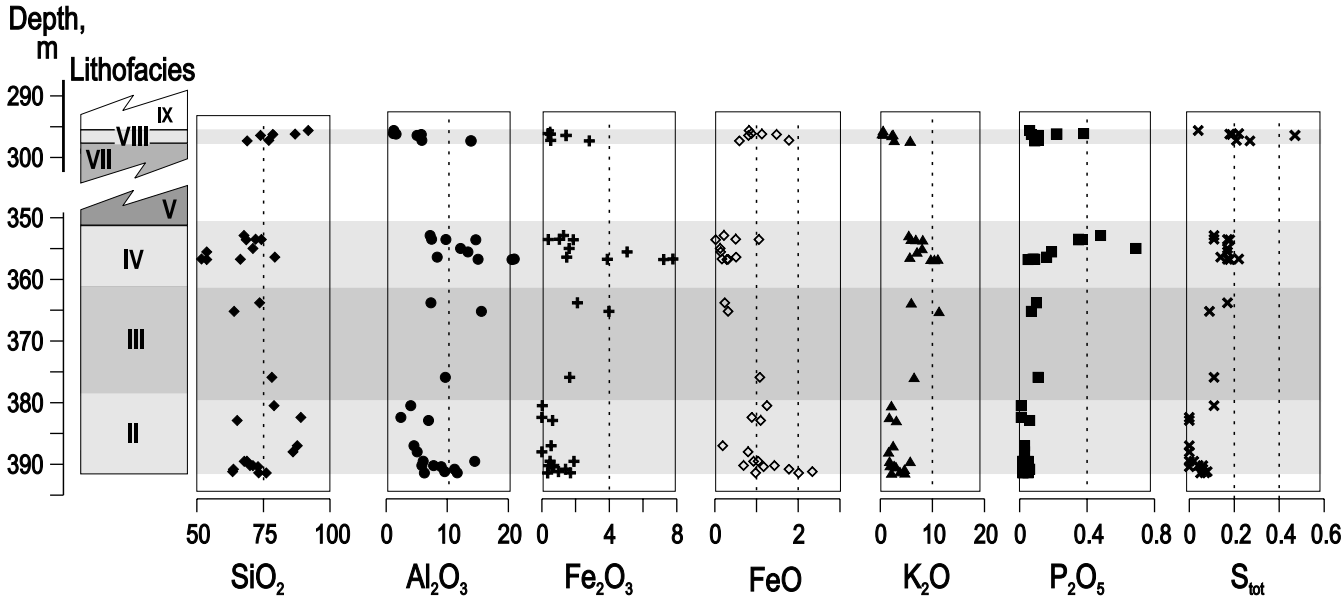

Figure 12 Chemical composition of clastic-dominated lithofacies plotted against stratigraphic height of the Kuetsjärvi Sedimentary Formation.

sandstones with a chlorite, tuffogenic matrix and carbonate breccias cemented by basaltic tuff and subsequent subaerial volcanism. The erupted volcanic material eventually buried the Kuetsjärvi basin and resulted in accumulation of a 2000-m-thick formation of alkaline volcanic rocks (Predovsky *et al.* 1974).

8. Implication for the Palaeoproterozoic global isotope shift of carbonate carbon

The 2330–2060 Ma positive carbon isotope excursion has been reported from a number of continents (reviewed in Melezhik *et al.* 1999), proving its global character (Baker & Fallick 1989a, b; Karhu & Holland 1996). It seems that, among reported ^{13}C-rich carbonates, those deposited in shallow-water environments dominate. This is the case for the Fennoscandian Shield (Karhu 1993; Melezhik *et al.* 1999, 2000), North America (Feng 1986; Melezhik *et al.* 1997a; Bekker & Eriksson 2003; Bekker *et al.* 2003) and India (Sreenivas *et al.* 1996). In some instances, ^{13}C-rich carbonates were precipitated in a shallow-water, restricted, marine environment (Tulomozero Formation; Melezhik *et al.* 1999, 2000, 2001) or in a shallow-water, restricted, lacustrine setting (Duitschland Formation; Buick *et al.* 1998). In many instances, high δ^{13}C carbonates are associated either with 'red beds' (Imandra/Varzuga and Pechenga Belts; Karhu & Melezhik 1992; Pokrovsky & Melezhik, 1995) or stromatolites (Lomagundi province; Schidlowski *et al.* 1976; Aravalli Supergroup; Sreenivas *et al.* 1996; Hutuo Group, Hua & Yongsheng 1997) or with both (Kona Dolomite; Feng 1986; Jatulian successions; Akhmedov *et al.* 1993; Melezhik *et al.* 1999, 2000, 2001; Labrador Trough; Melezhik *et al.* 1997a; Wyoming Craton; Bekker & Eriksson 2003; Bekker *et al.* 2003). Almost all reported that ^{13}C-rich carbonates are represented by dolomite, although calcite (Karhu 1993; Buick *et al.* 1998) and magnesite (Melezhik *et al.* 2001) have occasionally been observed. All these indicate that the studied ^{13}C-rich carbonates may not represent open marine environments, and therefore, their carbon isotopic composition may not always correspond to the isotopic composition of atmospheric CO_2 and bicarbonate of coeval open ocean.

The KSF dolostones, which record the 2330–2060 Ma isotopic signal of the carbonate carbon on the Fennoscandian Shield (Karhu 1993), represent non-marine carbonates, and therefore, their isotopic signal may or may not equate with the global δ^{13}C signal. The δ^{13}C global signal might have been modified by local factors associated with the Kuetsjärvi lake environment; namely, evaporation, enhanced biological uptake of ^{12}C, and penecontemporaneous oxidation of organic material in cyanobacterial mats. Hot-spring waters are another factor that could seriously have modified the composition of ambient lake water. The isotopic part of this

Figure 11 Core and outcrop photographs of Unit X. Core photographs denoted as drill hole X (DHX) with depth-in-core given in metres. (a) Vertical section through mottled, microbially laminated (stromatolitic) dolomicrite layers with flat, curly and blister laminae separated by thin, irregular partings of silica sinters (pale grey colours) (DHX 272·6); (b) Microbially laminated, dolomicrite deformed by enterolithic bedding and tepee structure (DHX 277·2); (c) Plane-polarised light photomicrograph showing stromatolitic dolomicrite (dark grey) with dolospar- and quartz-filled fenestrae (DHX 277·5); (d) Vertical section through iron-stained dolocrete with tepee-related deformation features and travertine-filled cracks (T) (related to opening of tepee) (DHX 271·6); (e) Vertical section through probable deformed enterolithic bedding in dolomicrites interlayered with silica sinters (S) and dolocrete (white). Note the possible verging tepee structure above the scale. The exposure is in the quarry 30 km southeast of DHX (Fig. 1); (f) Polished slab showing vertical section through dissolution cavity of surface origin in allochemical, sandy, micritic dolostone (D); cavity walls marked by reddening and silica sinter (S). The cavity is filled by sandy to fine-pebble dolostone conglomerate (C). These features indicate subaerial exposure. Sample collected from the quarry 30 km southeast of DHX (Fig. 1); (g) Plane-polarised light photomicrograph of probable sulphate micronodules pseudomorphed by dolospar in dolomicrite groundmass (DHX 275·5); (h) Polished slab showing vertical section through a tepee-like structure and associated deformation and buckling of dolomicrite layers. Finely laminated travertine (T) caps the dolomicrite and is itself capped by thin silica sinter which also fills downward tapering fractures. These features imply a period of emergence and influence of hydrothermal fluids. Sample collected in the quarry 30 km southeast of DHX (Fig. 1).

https://doi.org/10.1017/S0263593300001140 Published online by Cambridge University Press

Table 5 Chemical compositions of siliciclastic-dominated units of the Kuetsjärvi Sedimentary Formation (drill hole X) (wt.%): (–) below the detection limit of 0·01 for S_{tot} and 0·1 for C_{org}; (n.d.) not determined

Sample number	Lithology	SiO_2	TiO_2	Al_2O_3	Fe_2O_3	FeO	MnO	MgO	CaO	Na_2O	K_2O	H_2O+	H_2O-	CO_2	P_2O_5	C_{org}	S_{tot}
Unit VIII, mixed siliciclastic-dolostone*																	
295·6	Quartz sandstone	91·8	0·00	1·24	0·49	0·82	0·00	1·05	1·69	0·01	0·54	0·57	0·05	1·26	0·06	–	0·04
296·1	Quartz sandstone with dolomite matrix	78·8	0·00	1·17	0·37	0·88	0·03	3·32	6·45	0·14	0·36	0·51	0·09	7·27	0·38	n.d.	0·22
296·2	Quartz sandstone with dolomite matrix	86·9	0·04	1·60	0·50	1·13	0·01	2·23	2·63	0·03	0·59	1·21	0·25	2·38	0·22	–	0·18
296·25	Arkosic siltstone	78·5	0·29	5·73	0·52	1·48	0·01	4·75	1·83	0·10	2·44	2·49	0·26	1·31	0·07	–	0·19
296·4	Arkosic siltstone	73·9	0·22	5·03	1·43	0·81	0·01	4·80	4·07	0·12	2·21	2·20	0·26	4·15	0·11	–	0·47
297·2	Arkosic siltstone	77·0	0·28	5·82	0·52	1·78	0·01	4·72	1·83	0·20	2·69	2·76	0·51	1·36	0·11	–	0·21
297·3	Arkosic siltstone	68·9	0·38	13·9	2·81	0·59	0·02	3·62	0·25	0·06	5·75	3·01	0·16	0·13	0·09	–	0·27
Unit IV, siliciclastic-dominated																	
352·9	Sericitic siltstone, calcitised	67·7	0·09	7·17	1·28	0·22	0·05	2·38	7·65	0·09	5·46	1·20	0·17	5·48	0·48	–	0·10
353·5	Sericitic siltstone, calcitised	72·0	0·12	7·43	1·03	0·50	0·03	1·86	5·26	0·11	5·90	1·05	0·25	3·81	0·35	–	0·11
353·5a	Sericitic siltstone	74·2	0·18	9·76	0·38	1·06	0·02	2·53	1·68	0·14	6·82	1·16	0·14	0·99	0·37	–	0·19
353·5b	Sericitic siltstone	68·5	0·34	14·6	1·86	0·02	0·00	2·57	0·65	0·15	8·16	1·90	0·24	0·11	0·35	–	0·18
355·0	Sericitic siltstone	71·0	0·25	12·2	1·61	0·13	0·01	2·12	1·67	0·11	8·03	1·47	0·10	0·48	0·69	–	0·17
355·5b	Phlogopite siltstone	53·7	0·46	13·4	5·05	0·14	0·04	10·3	3·30	0·21	7·07	3·21	0·17	2·20	0·19	–	0·15
356·4	Sericitic siltstone	79·3	0·21	8·3	1·47	0·51	0·01	0·68	1·29	0·19	5·68	0·94	0·11	0·84	0·16	–	0·14
356·7a	Haematite, sericitic mudstones	66·3	0·47	15·0	3·88	0·32	0·01	1·55	0·19	0·21	9·70	2·18	0·29	0·09	0·09	–	0·16
356·7	Haematite, sericitic mudstones	51·7	0·70	21·0	7·77	0·17	0·01	3·13	0·30	0·14	11·1	3·09	0·12	0·17	0·08	–	0·22
356·7b	Haematite, sericitic mudstones	53·7	0·65	20·6	7·22	0·29	0·01	2·50	0·14	0·13	10·4	3·18	0·53	0·11	0·05	–	0·18
Unit III, siliciclastic-dominated																	
363·8	Arkosic sandstone, calcitised	73·5	0·19	7·31	2·10	0·24	0·12	0·30	5·11	0·17	5·95	0·37	0·15	3·95	0·10	–	0·17
365·2	Sericitic mudstone	64·0	0·48	15·6	3·97	0·32	0·02	1·35	0·22	0·45	11·3	1·54	0·24	0·10	0·07	–	0·09
375·9	Arkosic sandstone	78·1	0·17	9·67	1·64	1·08	0·01	0·46	0·30	0·20	6·49	0·82	0·23	0·18	0·11	–	0·12
380·5	Arkosic sandstone with dolomite matrix	79·0	0·11	4·01	0·02	1·25	0·03	2·40	5·22	0·06	2·14	1·21	0·13	4·03	0·01	–	0·13
382·4	Arkosic sandstone with calcite matrix	89·0	0·03	2·39	0·00	0·89	0·01	0·20	2·77	0·05	1·72	0·26	0·13	2·07	0·01	–	–
382·9	Arkosic sandstone with dolomite matrix	65·1	0·23	6·92	0·63	1·10	0·04	5·23	8·39	0·08	3·10	2·07	0·24	6·70	0·06	–	–
387·0	Arkosic sandstone	87·7	0·06	4·53	0·54	0·19	0·06	0·69	1·19	0·30	2·48	0·69	0·11	1·05	0·03	–	–
388·0	Fine-grained, arkosic, calcite-cemented sandstone	86·1	0·08	5·07	0·00	0·80	0·03	1·38	6·84	1·26	1·60	0·87	0·14	5·37	0·03	–	–
Unit II, mixed siliciclastic-dolostone*																	
389·50	Fine-grained, arkosic, calcite-cemented sandstone	68·76	0·11	6·05	0·48	1·04	0·04	1·87	10·13	1·17	1·79	1·37	0·17	7·38	0·02	–	–
389·52	Sericitic mudstone	67·78	0·40	14·48	1·90	0·93	0·01	4·06	0·57	0·50	5·75	2·64	0·21	0·35	0·05	–	0·02
389·54	Sericitic mudstone	67·84	0·34	14·58	1·81	0·97	0·01	3·83	0·32	1·07	5·57	2·76	0·28	0·23	0·04	–	0·04
390·2	Fine-grained, arkosic, calcite-cemented sandstone	69·92	0·09	5·83	0·70	0·69	0·04	1·66	9·02	1·27	1·89	1·38	0·16	7·08	0·02	–	0·04
390·22	Fine-grained, arkosic, calcite-cemented sandstone	71·04	0·15	7·76	0·39	1·43	0·03	2·44	6·36	0·80	2·64	1·80	0·25	5·00	0·02	–	0·06
390·4	Fine-grained, arkosic, calcite-cemented sandstone	72·92	0·17	9·00	0·59	1·17	0·02	2·20	4·35	1·00	3·02	1·85	0·30	3·25	0·04	–	–
390·8	Sericitic, dolomite-cemented mudstone	63·69	0·29	11·19	1·40	1·78	0·04	4·08	5·42	0·31	4·64	2·44	0·26	4·28	0·06	–	0·06
391·2	Fine-grained, arkosic, calcite-cemented sandstone	63·41	0·51	9·57	0·98	2·34	0·04	3·57	6·90	0·37	3·79	2·17	0·38	5·50	0·04	n.d.	0·08
391·4	Sericitic mudstone	73·17	0·28	11·61	1·69	0·98	0·01	3·30	0·58	0·32	4·73	2·29	0·20	0·45	0·05	–	0·07
391·42	Fine-grained, arkosic, calcite-cemented sandstone	76·03	0·11	6·24	0·34	2·01	0·03	2·38	4·61	1·09	2·17	1·32	0·28	3·14	0·02	–	0·05

*Interbedded carbonate rocks are characterised in Table 6.

Table 6 Chemical composition of mixed siliciclastic-dolostone and dolostone-dominated units of Kuetsjärvi Sedimentary Formation (drill hole X) (wt.%): (–) below detection limit of 0·1 for C_{org} and 0·01 for other elements; and (n.d.) not determined

Sample number	Lithology	SiO_2	Al_2O_3	Fe_2O_{3tot}	MnO♣	MgO♣	CaO♣	Na_2O	K_2O	P_2O_5	S_{tot}	C_{org}
Unit XI, mixed siliciclastic-dolostone*												
267·87	Sandy, sparry limestone with chlorite	39·8	2·96	1·84	0·14	3·84	26·3	0·02	0·14	0·26	0·05	n.d.
268·0	Sandy, sparry limestone with chlorite	53·5	2·65	1·11	0·08	4·59	18·9	0·008	0·022	0·07	0·03	n.d.
Shear zone carbonate rocks												
268·1	Sandy, sparry dolostone	32·9	1·23	1·05	0·11	16·1	26·7	–	–	0·06	n.d.	–
268·6	Sandy limestone	30·9	1·48	0·45	0·10	3·16	33·9	0·01	0·05	0·03	0·02	n.d.
Unit X, dolostone-dominated												
269·4	Interbedded micritic dolostone and laminated stromatolite	8·41	1·57	0·47	0·07	18·2	32·5	–	0·03	0·10	n.d.	n.d.
269·5	Sandy, sparry, allochemical dolostone	14·4	1·28	0·34	0·08	16·5	30·4	–	0·16	0·06	n.d.	n.d.
269·7	Sandy, sparry, allochemical dolostone with micronodules	13·3	1·36	0·28	0·08	17·3	28·0	–	0·17	0·07	0·02	–
269·9	Sandy, sparry, allochemical dolostone	25·4	1·47	0·40	0·04	15·3	26·1	–	0·049	0·06	0·02	n.d.
270·15	Interbedded pink, micritic dolostone and laminated stromatolite	7·87	0·98	0·28	0·07	21·3	31·0	–	0·03	0·09	n.d.	n.d.
270·7	Sandy, micritic dolostone with micronodules	13·2	2·26	0·38	0·06	16·2	28·9	–	0·46	0·09	n.d.	n.d.
271·1	Sandy, micritic dolostone with micronodules	14·3	2·74	0·55	0·05	14·1	30·2	–	0·66	0·09	n.d.	n.d.
271·5	Sandy, sparry, allochemical dolostone with micronodules	17·9	1·65	0·25	0·03	13·6	28·3	–	0·40	0·07	n.d.	n.d.
271·6	Sparry, allochemical dolostone	5·78	0·81	0·20	0·06	19·4	31·4	–	–	0·13	n.d.	n.d.
272·3	'Curly', laminated stromatolite	17·8	1·67	0·31	0·03	16·4	25·9	–	0·46	0·06	n.d.	n.d.
272·5	Sandy, micritic, dolostone with micronodules	12·6	2·75	0·45	0·03	17·9	27·0	–	0·72	0·08	n.d.	n.d.
272·7	Interbedded pink, micritic dolostone and white, sparry, allochemical dolostone	9·99	1·10	0·22	0·03	16·3	30·8	–	0·30	0·07	n.d.	n.d.
273·5	Sandy, micritic dolostone	16·5	1·72	0·32	0·02	16·6	26·0	–	0·54	0·06	n.d.	n.d.
273·7	Sandy, micritic dolostone	30·8	3·46	0·58	0·02	12·9	21·0	–	1·05	0·09	n.d.	n.d.
274·0	Sandy, laminated stromatolite	26·0	2·62	0·42	0·02	13·6	23·5	–	0·81	0·09	n.d.	n.d.
274·6	Sandy, sparry, allochemical dolostone	43·0	0·79	0·21	0·01	11·5	16·8	0·01	0·31	0·01	0·03	–
275·5	Sandy, micritic dolostone with micronodules	12·2	2·54	0·41	0·02	18·0	27·3	–	0·75	0·07	n.d.	n.d.
Unit X, dolostone-dominated												
276·7	Sandy, sparry, allochemical dolostone	13·4	1·56	0·22	0·01	17·9	26·9	–	0·44	0·07	n.d.	n.d.
277·1	Sandy, laminated stromatolite	27·5	2·83	0·51	0·03	14·1	22·1	–	0·86	0·12	n.d.	n.d.
277·2	Sandy, laminated stromatolite	28·5	2·24	0·66	0·02	14·5	20·2	0·02	0·95	0·06	0·03	–
277·5	Sandy, laminated stromatolite	19·5	3·34	0·53	0·03	15·5	24·7	–	0·97	0·16	n.d.	n.d.
278·0	Sandy, micritic stromatolite	13·1	1·31	0·30	0·03	17·7	27·7	–	0·39	0·10	n.d.	n.d.
Unit IX, dolostone-dominated												
278·8	Recrystallised, sandy dolostone	25·7	1·91	0·38	0·03	13·6	23·7	–	0·59	0·15	n.d.	n.d.
279·5	Sandy, sparry, allochemical dolostone	12·2	0·96	0·22	0·02	17·8	28·0	–	0·57	0·07	n.d.	n.d.
282·3	Sandy, sparry, allochemical dolostone	30·2	3·05	0·58	0·03	12·8	21·6	–	0·96	0·14	n.d.	n.d.
283·0	Sandy, sparry, allochemical dolostone	33·7	1·28	0·42	0·03	12·1	22·1	0·22	0·46	0·07	n.d.	n.d.
283·5	Sandy, sparry dolostone	36·4	1·37	0·27	0·02	11·7	19·3	–	0·70	0·08	n.d.	n.d.
283·7	Sandy, sparry dolostone	37·0	1·51	0·28	0·03	11·5	20·2	–	0·71	0·09	n.d.	n.d.
284·5	Sandy, sparry dolostone	30·2	1·57	0·29	0·03	12·4	22·4	–	0·79	0·12	n.d.	n.d.
285·7	Sandy, sparry dolostone	47·4	0·30	0·23	0·02	10·3	17·0	0·01	0·11	0·01	0·15	–
Shear zone carbonate rocks												
290·5	Brecciated, sandy, micritic limestone	12·9	0·89	0·24	0·14	2·5	41·8	0·12	0·63	0·10	n.d.	n.d.
293·0	Brecciated, sandy, micritic dolostone	18·2	1·24	0·54	0·06	14·7	26·7	–	0·67	0·13	n.d.	n.d.
293·1	Sandy, micritic dolostone	20·2	1·50	0·54	0·05	15·0	25·6	–	0·64	0·12	n.d.	n.d.
295·0	Sandy, sparry dolostone	29·9	2·31	1·04	0·08	14·5	20·6	–	0·62	0·29	n.d.	n.d.
295·3	Sandy, sparry limestone	30·2	1·17	0·76	0·05	14·4	20·6	0·02	0·51	0·33	0·04	–
Unit VIII, mixed siliciclastic-dolostone*												
296·5	Carbonate conglomerate	31·0	2·73	1·60	0·08	13·5	20·7	0·2	0·58	0·32	n.d.	n.d.
296·54	Carbonate conglomero-breccia	26·4	2·36	1·42	0·05	14·1	11·9	0·21	0·52	0·75	0·04	–
296·56	Carbonate conglomerate	43·8	2·86	1·25	0·04	11·2	15·1	0·16	0·99	0·18	0·23	–
Unit VIII, mixed siliciclastic-dolostone*												
297·4	Carbonate breccia	35·8	3·15	1·67	0·06	11·3	19·8	–	0·60	0·74	n.d.	n.d.
Unit VII, dolostone-dominated												
297·7	Sandy, micritic, allochemical dolostone	19·3	1·49	1·24	0·06	17·0	24·1	–	0·421	1·19	0·01	–
298·4	Micritic dolostone with pseudomorphed evaporite crust	9·87	0·68	0·62	0·07	17·5	29·1	–	0·57	0·25	n.d.	n.d.

https://doi.org/10.1017/S0263593300001140 Published online by Cambridge University Press

Table 6 *Continued*

Sample number	Lithology	SiO_2	Al_2O_3	Fe_2O_{3tot}	MnO♣	MgO♣	CaO♣	Na_2O	K_2O	P_2O_5	S_{tot}	C_{org}
300·2	Sandy, micritic, allochemical dolostone with travertine crust	10·5	1·04	0·26	0·03	18·2	28·4	–	0·46	0·13	n.d.	n.d.
300·4	Sandy, micritic, stromatolitic dolostone with travertine crust	15·4	0·45	0·21	0·03	17·2	26·6	–	0·23	0·15	n.d.	n.d.
301·4	Micritic, stromatolitic dolostone	3·95	0·57	0·34	0·02	20·1	28·6	0·02	0·35	0·14	0·02	–
301·45	Sandy, micritic, stromatolitic dolostone	38·4	2·32	0·25	0·02	12·4	17·1	0·02	1·38	0·11	0·02	–
301·7	Sandy, micritic, allochemical dolostone	17·3	2·69	0·37	0·03	16·7	24·7	–	1·52	0·07	n.d.	n.d.
302·4	Micritic, allochemical dolostone	8·77	0·63	0·26	0·03	18·9	28·9	–	0·29	0·08	n.d.	n.d.
303·4	Sandy, micritic, allochemical dolostone with micronodules	10·6	0·82	0·20	0·02	18·7	27·9	–	0·49	0·08	n.d.	n.d.
304·0	Sandy, micritic, stromatolitic dolostone with travertine crust	15·8	1·06	0·27	0·02	17·2	26·2	–	0·41	0·08	n.d.	n.d.
305·0	Micritic, stromatolitic dolostone	2·84	0·53	0·15	0·02	20·8	31·6	–	0·19	0·08	n.d.	n.d.
306·3	Micritic, stromatolitic dolostone	4·14	0·22	0·11	0·02	20·2	31·0	–	0·16	0·07	n.d.	n.d.
306·9	Interbedded, micritic, allochemical dolostone and stromatolitic dolostone	5·20	0·71	0·21	0·03	19·8	30·8	–	0·29	0·15	n.d.	n.d.
307·3	Micritic, stromatolitic dolostone with travertine crust	1·63	–	0·08	0·02	21·1	32·3	–	0·06	0·09	n.d.	n.d.
308·9	Dolostone breccia	7·96	1·40	0·27	0·02	19·2	29·2	–	0·47	0·08	n.d.	n.d.
309·7	Sandy, micritic, stromatolitic dolostone	14·1	2·05	0·29	0·02	17·1	26·6	–	0·95	0·17	n.d.	n.d.
309·9	Sandy, micritic, allochemical dolostone	21·4	2·34	0·38	0·04	15·8	23·4	0·18	0·96	0·18	n.d.	n.d.
310·2	Sandy, micritic dolostone	14·7	0·27	0·32	0·02	17·8	26·2	0·02	0·05	0·03	0·13	–
310·25	Micritic dolostone	0·48	0·30	0·64	0·02	21·4	30·8	0·02	0·11	0·07	0·07	–
311·7	Interbedded allochemical and stromatolitic dolostone	17·5	1·01	0·20	0·02	17·3	25·7	–	0·50	0·08	n.d.	n.d.
314·5	Micritic, stromatolitic dolostone	0·63	–	0·09	0·02	21·8	32·7	–	0·05	0·10	n.d.	n.d.
314·9	Sandy, micritic dolostone	21·4	0·95	0·19	0·03	15·4	24·2	–	0·43	0·14	n.d.	n.d.
315·1	Sandy, micritic, allochemical dolostone	25·8	0·98	0·18	0·03	14·2	23·3	–	0·44	0·15	n.d.	n.d.
Unit VII, dolostone-dominated												
316·6	Interbedded sandy, micritic and sparry dolostone	17·1	1·43	0·22	0·03	17·0	25·4	–	0·26	0·09	n.d.	n.d.
316·9	Interbedded sandy, sparry, and micritic, stromatolitic dolostone	27·8	1·25	0·21	0·02	14·0	22·7	–	0·15	0·20	n.d.	n.d.
317·0	Flat-pebble conglomero-breccia	20·6	1·41	0·22	0·03	16·0	25·1	–	0·17	0·15	n.d.	n.d.
317·1	Micritic, stromatolitic, dolostone	1·79	0·17	0·16	0·03	21·5	32·4	–	0·07	0·10	n.d.	n.d.
317·8	Sandy, micritic, allochemical, dolostone with micronodules	12·3	0·64	0·19	0·03	17·1	28·1	–	0·14	0·09	n.d.	n.d.
320·5	Micritic, stromatolitic dolostone with dolomite pseudomorphed evaporite crust	3·81	0·08	0·12	0·03	19·0	33·0	–	0·06	0·12	n.d.	n.d.
321·0	Sandy, micritic dolostone with micronodules	11·3	0·38	0·12	0·02	17·0	29·2	–	0·15	0·15	n.d.	n.d.
322·0	Sandy, micritic dolostone with micronodules	19·8	0·61	0·13	0·02	16·9	25·0	–	0·16	0·07	n.d.	n.d.
322·5	Micritic, stromatolitic dolostone	–	–	0·12	0·03	21·5	33·3	–	0·02	0·12	n.d.	n.d.
322·6	Micritic, stromatolitic dolostone	–	–	0·12	0·03	22·4	33·0	–	0·02	0·10	n.d.	n.d.
322·7	Micritic dolostone	1·02	0·26	0·17	0·02	22·9	29·8	–	0·05	0·12	0·17	–
326·2	Sandy, micritic, allochemical dolostone with micronodules	21·4	0·69	0·20	0·03	15·8	24·7	–	0·16	0·11	n.d.	n.d.
327·7	Sandy, micritic dolostone	11·3	0·62	0·15	0·04	16·7	29·8	–	0·32	0·12	n.d.	n.d.
329·3	Sandy, allochemical dolostone	15·7	0·83	0·17	0·05	n.d.	n.d.	–	0·60	0·08	n.d.	n.d.
332·5	Micritic, stromatolitic dolostone with travertine crust	8·94	0·10	0·16	0·05	n.d.	n.d.	–	0·09	0·11	n.d.	n.d.
334·3	Sandy, micritic dolostone	16·5	0·75	0·15	0·02	n.d.	n.d.	–	0·31	0·09	n.d.	n.d.
335·3	Micritic dolostone	9·44	0·29	0·22	0·01	20·0	28·1	–	0·14	0·06	0·01	–
Unit VI, dolostone-dominated												
336·2	Sandy, sparry dolostone with travertine crust	30·4	0·65	0·30	0·01	14·5	20·7	0·02	0·33	0·02	0·11	–
336·25	Sandy, sparry dolostone	26·3	0·38	0·28	0·02	15·1	22·6	0·02	0·15	0·04	0·11	–
337·4	Sandy, sparry dolostone	19·6	0·64	0·32	0·03	15·1	27·3	–	0·36	0·04	0·03	–
337·46	Sandy, sparry dolostone	40·3	0·79	0·22	0·02	10·7	19·4	0·01	0·62	0·01	0·02	–
339·4	Micritic dolostone	0·65	0·03	0·10	0·02	21·3	32·8	–	0·06	0·13	n.d.	n.d.
340·3	Micritic dolostone	2·93	0·01	0·10	0·03	21·5	31·7	–	0·04	0·09	n.d.	n.d.
342·5	Sandy, sparry dolostone	16·9	1·65	0·23	0·04	16·9	26·0	–	0·47	0·06	n.d.	n.d.

https://doi.org/10.1017/S0263593300001140 Published online by Cambridge University Press

Table 6 *Continued*

Sample number	Lithology	SiO_2	Al_2O_3	Fe_2O_{3tot}	MnO♣	MgO♣	CaO♣	Na_2O	K_2O	P_2O_5	S_{tot}	C_{org}
Unit VI, dolostone-dominated												
342·8	Micritic dolostone	0·58	0·08	0·14	0·03	22·6	32·5	–	0·08	0·09	n.d.	n.d.
343·2	Sparry, allochemical dolostone	7·61	0·73	0·27	0·05	11·2	37·5	–	0·06	0·06	n.d.	n.d.
343·3	Sparry, allochemical limestone	8·50	0·71	0·26	0·05	9·69	38·6	0·1	0·05	0·05	n.d.	n.d.
343·6	Sandy, sparry, dolostone	31·6	2·21	0·59	0·02	10·8	24·6	–	0·51	–	0·09	–
Unit V, mixed siliciclastic-dolostone*												
344·7	Sandy, micritic dolostone	27·4	2·31	0·24	0·03	14·6	21·9	0·14	0·99	0·06	n.d.	n.d.
346·4	Sandy, sparry, allochemical dolostone	19·5	1·30	0·30	0·06	13·6	27·5	–	0·45	0·07	n.d.	n.d.
349·3	Micritic, allochemical dolostone	5·43	0·89	0·72	0·15	19·6	30·4	–	0·47	0·09	n.d.	n.d.
Unit IV, mixed siliciclastic-dolostone*												
355·5	Sandy, sparry limestone	28·5	4·92	1·53	0·15	9·93	27·2	0·08	2·05	0·61	0·17	–
355·55	Sandy, sparry limestone	43·6	4·76	1·26	0·11	5·28	22·7	0·29	1·24	0·31	0·14	–
357·1	Sandy, sparry dolostone	26·3	4·10	1·80	0·24	12·7	27·0	0·04	1·59	0·30	0·06	–
Unit II, mixed siliciclastic-dolostone*												
380·9	Sandy, micritic, allochemical dolostone	18·6	1·82	0·70	0·13	16·2	25·9	–	0·83	0·07	n.d.	n.d.
381·1	Flat-pebble conglomerate	36·4	1·28	0·48	0·02	13·8	18·0	0·01	0·51	0·12	0·07	–
381·2	Sandy, micritic, allochemical dolostone	41·2	3·40	0·83	0·02	11·9	16·4	0·05	1·89	0·03	0·09	–
381·4	Sandy, micritic, allochemical dolostone	25·1	2·23	0·84	0·14	14·3	23·6	–	0·90	0·09	n.d.	n.d.
381·55	Flat-pebble conglomerate	25·1	1·76	0·63	0·12	13·9	24·8	–	0·83	0·07	n.d.	n.d.
381·6	Sandy, micritic, allochemical dolostone	24·3	2·27	0·87	0·11	12·0	25·9	–	1·04	0·08	n.d.	n.d.
382·0	Sandy, micritic, allochemical dolostone	21·5	1·86	0·70	0·17	12·6	26·2	–	0·93	0·09	n.d.	n.d.
382·1	Sandy, micritic, allochemical dolostone	30·4	1·02	0·31	0·08	10·6	25·3	0·03	0·65	0·02	n.d.	–
384·8	Recrystallised, sandy dolostone	33·4	2·52	0·63	0·05	11·5	26·4	0·02	1·24	0·03	n.d.	–
386·1	Recrystallised, sandy dolostone	30·8	5·47	1·51	0·06	13·1	23·1	0·03	2·81	0·05	n.d.	–
387·6	Recrystallised, sandy dolostone	27·1	5·08	1·24	0·06	14·4	25·0	0·02	1·58	0·05	0·02	–

*Interbedded clastic rocks are characterised in Table 5.
♣Acid-soluble MnO, MgO and CaO contents were determined by ICP-AES.

problem will be considered in a companion paper (Melezhik *et al*. 2005).

9. Summary and conclusions

The KSF is a c. 150-m-thick siliciclastic-carbonate succession accumulated between 2330 and 2060 Ma ago in a braidplain/delta and lacustrine environment within a Palaeoproterozoic intracontinental rift. The succession consists of the lower Quartzite and upper Dolostone members, which can be subdivided into 11 siliciclastic-dominated, mixed siliciclastic–dolostone and dolostone-dominated units.

The succession exhibits many characteristics of non-marine and lacustrine sediments. It rests on a palaeo-weathering crust and is sealed between two subaerially erupted volcanic formations. It exhibits rapid variation of sedimentary facies in vertical section marked by abundant flat-laminated microbial mats, 'red beds', variegated and mottled rocks, travertines, surface silicification, and dissolution cavities infilled with fine-grained clastic material. All carbonate lithologies are highly impure, sandy dolostones. In addition, the KSF rocks lack tidal or other shallow marine features.

The lake was infilled during three successive depositional phases. The initial phase was marked by accumulation of siliciclastic-dominated, and mixed, siliciclastic–dolostone lithofacies in fluviatile-shoreline and shallow-water lacustrine settings under oxic conditions. Carbonates were precipitated inorganically on a ponded shoreline environment. The second phase was marked by biologically induced precipitation of dolomite during lowstands when playa-like conditions existed across major parts of the basin. The precipitation of carbonates was additionally promoted by an arid to semi-arid climate. Ambient lake waters were influenced by hydrothermal springs, which led to the formation of abundant travertines. The terminal phase was manifested by renewed rift propagation and voluminous volcanic eruptions.

The lake experienced several phases of emergence and submergence marked by formation of dolocretes, silcretes and solution surfaces. The rocks were affected by post-sedimentary infiltration of reducing, H_2S-free fluids, resulting in bleaching and discoloration of 'red beds'. Subsequently, the rocks underwent greenschist facies metamorphism caused by the c. 1850 Ga Svecofennian orogeny.

10. Acknowledgements

The present article reports the results obtained by the international research group working in the framework of a project entitled 'World-wide 2 billion-year-old positive carbon isotopic excursion: the evolutionary significance and driving forces'. This research has been supported by INTAS-RFBR 95–928. The fieldwork has been financed by the IGCP project 408 and the Geological Survey of Norway, project 282200. The Scottish Universities Environmental Research Centre has been supported by the Consortium of Scottish Universities and the Natural Environment Research Council. We thank the Carnegie Trust for the Universities of Scotland for financial support towards the cost of colour plates. Access to core material of the Central Kola Prospecting Expedition is acknowledged with thanks. We are grateful to F. Mitrofanov for permission to use the sample collection from the Pechenga Belt and unpublished analytical data on C abundances. A. Siedlecka is acknowledged for stimulating discussion and constructive criticism of the manuscript and illustrations.

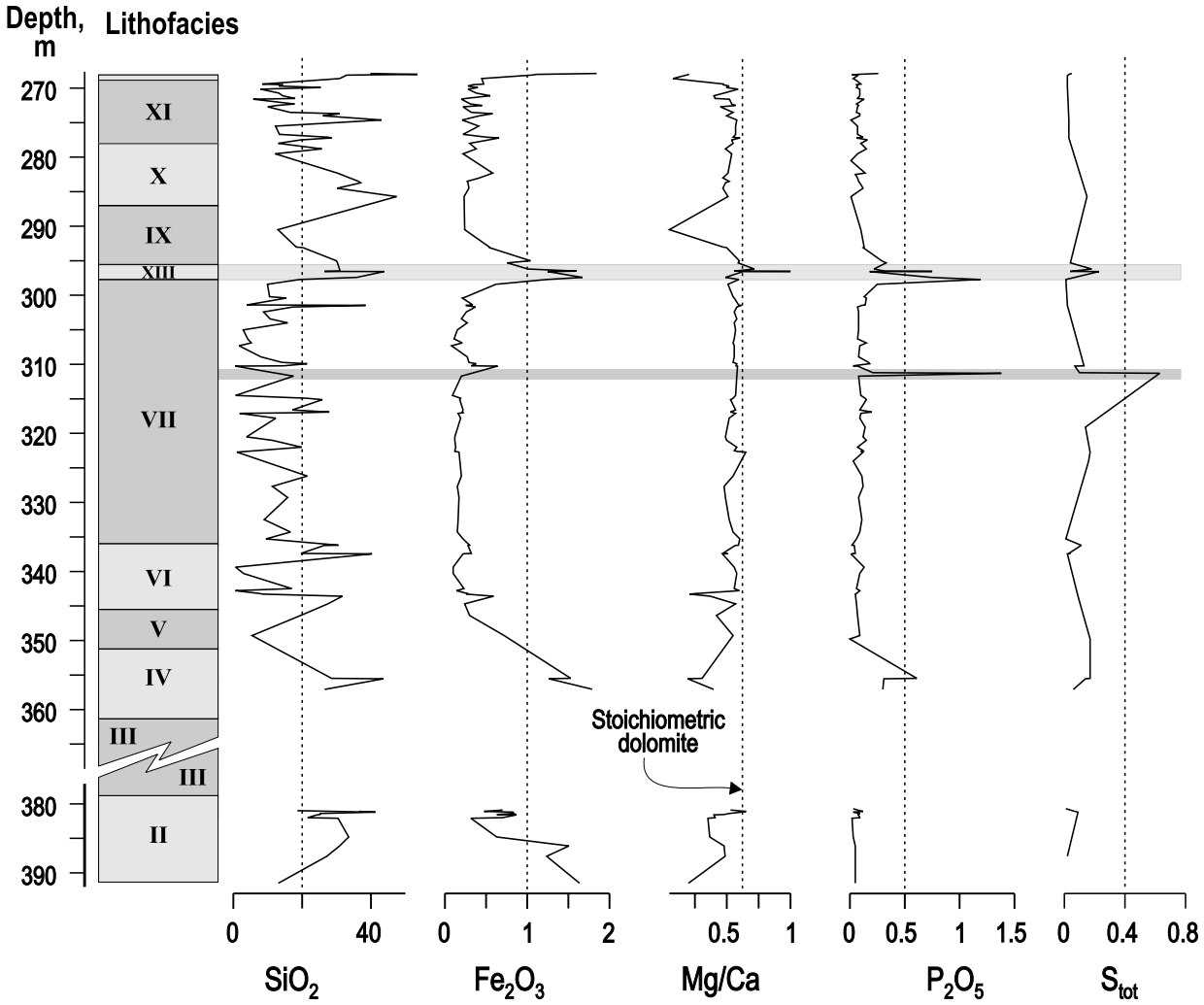

Figure 13 Chemical composition of mixed clastic-dolostone and dolostone-dominated units plotted against stratigraphic height of the Kuetsjärvi Sedimentary Formation. Grey bars indicate beds enriched in phosphorous and sulphur.

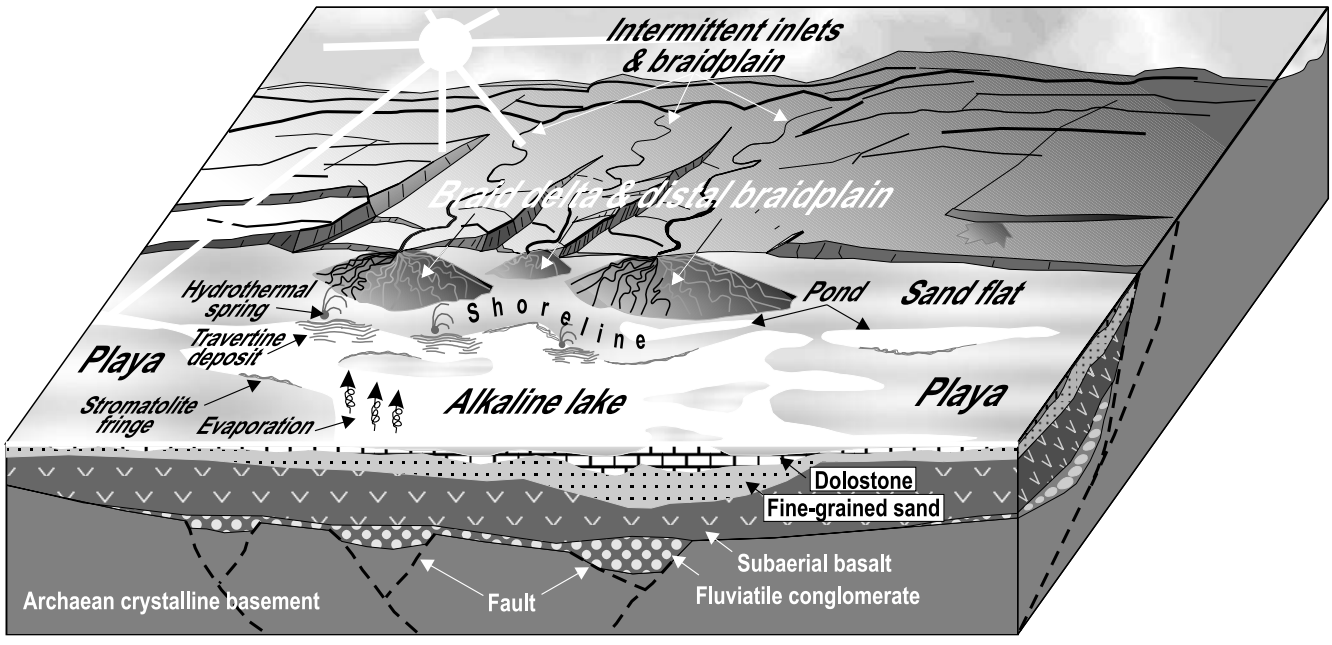

Figure 14 Reconstruction of the Kuetsjärvi rift-related lake.

https://doi.org/10.1017/S0263593300001140 Published online by Cambridge University Press

Official referees A. Prave and M. Talbot are thanked for their constructively critical reviews and for their effort to make the manuscript intelligible.

11. References

Akhmedov, A. M., Krupenik, V. A., Makarikhin, V. V. & Medvedev, P. V. 1993. *Carbon isotope composition of carbonates in the early Proterozoic sedimentary basins.* Printed report. Petrozavodsk: Institute of Geology of the Karelian Scientific Centre. [In Russian.]

Alonso-Zarza, A. M. 2003. Palaeoenvironmental significance of palustrine carbonates and calcretes in the geological record. *Earth-Science Reviews* **60**, 261–98.

Amelin, Yu. V., Heaman, L. M. & Semenov, V. S. 1995. U-Pb geochronology of layered mafic intrusions in the eastern Baltic Shield: implications for the timing and duration of Palaeoproterozoic continental rifting. *Precambrian Research* **75**, 31–46.

Atabey, E., Atabey, N. & Kara, H. 1998. Sedimentology of caliche (calcrete) occurrences of the Kirşehir region. *Mineral Research and Exploration Bulletin* **120**, 69–80.

Baker, A. J. & Fallick, A. E. 1989a. Evidence from Lewisian limestone for isotopically heavy carbon in two-thousand-million-year-old sea water. *Nature* **337**, 352–54.

Baker, A. J. & Fallick, A. E. 1989b. Heavy carbon in two-billion-year-old marbles from Lofoten-Vesterålen, Norway: implications for the Precambrian carbon cycle. *Geochimica et Cosmochimica Acta* **53**, 1111–15.

Bakushkin, Ye. M. & Akhmedov, A. M. 1975. Basal conglomerate of the Pechenga Complex near the Mt. General'skaya. *In* Bel'kov, I. V. (ed.) *Geology and geochemistry of the metamorphic complexes of the Kola Peninsula*, 70–7. Apatity: Kola Science Centre. [In Russian.]

Balashov, Yu. A. 1996. Geochronology of Early Proterozoic rocks from the Pechenga/Varzuga structure in the Kola Peninsula. *Petrology* **4**, 3–25. [In Russian.]

Beauchamp, B., Oldershaw, A. E. & Krouse, R. 1987. Upper Carboniferous to Upper Permian ^{13}C-enriched primary carbonates in the Sverdrup Basin, Canadian Arctic: comparisons to coeval western North American ocean margins. *Chemical Geology* **65**, 391–413.

Behr, H.-J. 2002. Magadiite and Magadi chert: a critical analysis of the silica sediments in the lake Magadi basin, Kenya. *In* Renaut, R. W. & Asley, G. M. (eds) Sedimentation in continental rifts. *Special Publication of the Society of Economic Paleontologists and Mineralogists* **73**, 257–73.

Behr, H.-J., Ahrendt, H., Martin, H., Porada, H., Röhrs, J. & Weber, K. 1983. Sedimentology and mineralogy of Upper Proterozoic playa-lake deposits in the Damara Orogen. *In* Martin, H and Eder, F. W. (eds) *Intracontinental fold belts*, 577–610. Berlin-Heidelberg: Springer-Verlag.

Bekker, A. Karhu, J. A., Eriksson, K. A. & Kaufman, A. J. 2003. Chemostratigraphy of Palaeoproterozoic carbonate successions of the Wyoming Craton: tectonic forcing of biogeochemical change? *Precambrian Research* **120**, 279–325.

Bekker, A. & Eriksson, K. A. 2003. A Palaeoproterozoic drowned carbonate platform on the southeastern margin of the Wyoming Craton: a record of the Kenorland breakup. *Precambrian Research* **120**, 327–64.

Brunskill, G. J. 1969. Fayetteville Green Lake, New York: Part 2: Precipitation and sedimentation of calcite in a meromictic lake with laminated sediments. *Limnology and Oceanography* **14**, 830–47.

Buick, I. S., Uken, R., Gibson, R. L. & Wallmach, T. 1998. High-δ^{13}C Paleoproterozoic carbonates from the Transvaal Supergroup, South Africa. *Geology* **26**, 875–8.

Calvo, J. P., Gomez, G. D., Alonso-Zarza, A. M. & Jimenez, S. 2000. Architecture of a bench-type carbonate lake margin and its relation to fluvially dominated deltas, Las Minas Basin, upper Miocene, Spain. *Journal of Sedimentary Research* **70**, 240–54.

Camoin, G., Casanova, J., Rouchy, J.-M., Blanc-Valleron, M.-M. & Deconinck, J.-F. 1997. Environmental control on perennial and ephemeral carbonate lakes: the central palaeo-Andean Basin of Bolivia during Late Cretaceous to early Tertiary times. *Sedimentary Geology* **113**, 1–26.

Capo, R. C., Whipkey, C. E., Blachère, J. R. & Chadwick, O. A. 2000. Pedogenic origin of dolomite in a basaltic weathering profile, Kohala peninsula, Hawaii. *Geology* **28**, 271–4.

Castle, J. W. 1990. Sedimentation in Eocene Lake Uinta (Lower Green River Formation), Northeastern Uinta Basin, Utah. *In* Katz, B. J. (ed.) Lacustrine basin exploration. *American Association of Petroleum Geologists Memoir* **50**, 243–63.

Chafetz, H. S., Rush, P. F. & Utech, N. M. 1991. Microenvironmental controls on mineralogy and habit of $CaCO_3$ precipitates: an example from an active travertine system. *Sedimentology* **38**, 107–26.

Chough, S. K., Hwang, I. G. & Choe, M. Y. 1990. The Miocene Doumsan fan-delta, Southeast Korea; a composite fan-delta system in back-arc margin. *Journal of Sedimentary Petrology* **60**, 445–55.

Cohen, A. S., Talbot, M. R., Awramik, S. M., Dettman, D. L. & Abell, P. 1997. Lake level and paleoenvironmental history of Lake Tanganyika, Africa, as inferred from late Holocene and modern stromatolites. *Geological Society of America Bulletin* **109**, 444–60.

Coleman, J. M. & Prior, D. B. 1982. Deltaic environments. *In* Scholle, P. A. & Spearing, D. (eds) *Sandstone depositional environments*, 139–78. Tusla, OK: American Association of Petroleum Geologists.

Demicco, R. V. & Hardie, L. A. 1994. Sedimentary structure and early diagenetic features of shallow marine carbonate deposits. *Society of Economic Paleontologists and Mineralogists Atlas Series* **1**. Tulsa, OK: Society of Economic Paleontologists and Mineralogists.

Elliott, T. 1986. Deltas. *In* Reading, H. G. (ed.) *Sedimentary environments and facies*, 113–54. Oxford: Blackwell Scientific Publications.

El-Tabakh, M., Riccioni, R. & Schreiber, C. 1997. Evolution of late Triassic rift basin evaporites (Passaic Formation): Newark Basin, Eastern North America. *Sedimentology* **44**, 767–90.

Eriksson, K. A. & Simpson, E. L. 2000. Quantifying the oldest tidal record; the 3.2 Ga Moodies Group, Barberton greenstone belt, South Africa. *Geology* **28**, 831–4.

Eriksson, K. A. & Simpson, E. L. 2002. Precambrian tidalites: recognition and significance (Abstract). *In 16th International Sedimentological Congress*, 92. Johannesburg: Rand Afrikaans University.

Evans, J. E. & Welzenbach, L. C. 1998. Episodes of carbonate deposition in a siliciclastic-dominated fluvial sequence, Eocene-Oligocene White River Group, South Dakota and Nebraska. *Geological Society of America Special Paper* **325**, 93–116.

Feng, J. 1986. Sulfur and oxygen isotope geochemistry of Precambrian marine sulfate and chert. Unpublished M.Sc. thesis, Northern Illinois University, Chicago, Illinois.

Freytet, P. 1973. Petrography and paleo-environment of continental carbonate deposits with particular reference to the upper Cretaceous and lower Eocene of Languedoc (southern France). *Sedimentary Geology* **10**, 25–60.

Gierlowski-Kordesch, E. H. 1998. Carbonate deposition in an ephemeral siliciclastic alluvial system: Jurassic Shuttle Meadow Formation, Newark Supergroup, Hartford Basin, USA. *Palaeogeography, Palaeoclimatology, Palaeoecology* **140**, 161–84.

Glover, B. W. & O'Beirne, A. M. 1994. Anatomy, hydrodynamics and depositional setting of a Westphalian C lacustrine delta complex, West Midlands, England. *Sedimentology* **41**, 115–32.

Grotzinger, J. P. 1989. Facies and evolution of Precambrian carbonate depositional systems: emergence of the modern platform archetype. *In* Crevello, P. D., Wilson, J. L., Sarg, J. F. & Read J. F. (eds) *Controls on carbonate platform and basin developments. Society of Economic Paleontologists and Mineralogists Special Publication* **44**, 79–106.

Guo, L. & Riding, R. 1992. Aragonite laminae in hot water travertine crusts, Rapolano, Italy. *Sedimentology* **39**, 1067–79.

Hanski, E., Huhma, H., Smol'kin, V. F. & Vaasjoki, M. 1990. The age of ferropicritic volcanites and comagmatic Ni-bearing intrusions at Pechenga, Kola Peninsula, U.S.S.R. *Geological Society of Finland Bulletin* **62**, 123–33.

Higgs, R. 1990. Sedimentology and tectonic implications of Cretaceous fan-delta conglomerates, Queen Charlotte Islands, Canada. *Sedimentology* 37, 83–103.

Horton, B. K. & Schmitt, J. G. 1996. Sedimentology of a lacustrine fan-delta system, Miocene Horse Camp Formation, Nevada, USA. *Sedimentology* **43**, 133–55.

Hua, Z. & Yongsheng, M. 1997. Carbon isotope stratigraphy of dolomites in the Early Proterozoic succession, north China. *Geological Magazine* **134**, 763–70.

Hyne, N. J., Cooper, W. A. & Dickey, P. A. 1979. Stratigraphy of intermontane, lacustrine delta, Catatumbo River, Lake Maracaibo, Venezuela. *Bulletin of the American Association of Petroleum Geologists* **63**, 2042–57.

Jones, B., Renaut, R. W. & Rosen, M. R. 1996. High-temperature (>90°C) calcite precipitation at Waikite Hot Springs, North Island, New Zealand. *Journal of the Geological Society of London 153, 481–96.*

Jones, B., Rosen, M. R. & Renaut, R. W. 1997. Silica-cemented beachrock from Lake Taupo, North Island, New Zealand. *Journal of Sedimentary Research* **67**, 805–14.

Jones, B., Renaut, R. W. & Rosen, M. R. 1998. Microbial biofacies in hot-spring sinters: a model based on Ohaaki Pool, North Island, New Zealand. *Journal of Sedimentary Research* **68**, 413–34.

Jones, B. & Renaut, R. W. 1996. Morphology and growth of aragonite crystals in hot-spring travertines at Lake Bogoria, Kenya Rift Valley. *Sedimentology* **43**, 323–40.

Jones, B. & Renaut, R. W. 1997. Formation of silica oncoids around geysers and hot springs at El Tatio, northern Chile. *Sedimentology* **44**, 287–304.

Kah, L. C & Knoll, A. H. 1996. Microbenthid distribution of Proterozoic tidal flats: Environmental and taphonomic considerations. *Geology* **24**, 79–84.

Karhu, J. A. 1993. Palaeoproterozoic evolution of the carbon isotope ratios of sedimentary carbonates in the Fennoscandian Shield. *Geological Survey of Finland Bulletin* **371**, 1–87.

Karhu, J. A. & Holland, H. D. 1996. Carbon isotopes and the rise of atmospheric oxygen. *Geology* **24**, 867–79.

Karhu, J. A. & Melezhik, V. A. 1992. Carbon isotope systematics of early Proterozoic sedimentary carbonates in the Kola Peninsula, Russia: Correlations with Jatulian formations in Karelia. *In* Balagansky, V. V. & Mitrofanov F. P. (eds) *Correlations of Precambrian formations of the Kola-Karelia region and Finland*, 48–53. Apatity: Kola Scientific Centre of the Russian Academy of Sciences.

Kinsman, D. J. J. & Park, R. K. 1976. Algal belt and coastal sabkha evolution, Trucial Coast, Persian Gulf. *In* Walter, M. R. (ed.) *Stromatolites*, 421–33. Amsterdam: Elsevier.

Klenova, M. V. 1968. Caspian Sea. *In* Fairbridge, R. W. (ed.). *The encyclopedia of geomorphology*, 109–16. New York, NY: Reinhold.

Knauth, L. P., Brilli, M. & Klonowski, S. 2003. Isotope geochemistry of caliche developed on basalt. *Geochimica et Cosmochimica Acta* **67**, 185–95.

Lowe, D. R. 1982. Sediment gravity flows: II. Depositional models with special reference to the deposits of high-density turbidity currents. *Journal of Sedimentary Petrology* **52**, 279–97.

Lybtsov, V. V. 1979. Stromatolites of the Palaeoproterozoic Pechenga Complex, Kola Peninsula. *Transactions of the USSR Academy of Sciences* **247**, 419–21. [In Russian.]

Marker, M. 1985. Early Proterozoic (c. 2000–1900 Ma) crustal structure on the north-eastern Baltic Shield: tectonic division and tectogenesis. *Norges geologiske undersøkelse Bulletin* **403**, 55–74.

Martel, A. T. & Gibling, M. R. 1991. Wave-dominated lacustrine facies and tectonically controlled cyclicity in the Lower Carboniferous Horton Bluff Formation, Nova Scotia, Canada. *In* Anadón, P., Cabrera, L. & Kelts, K. (eds) *Lacustrine facies analysis. Special Publication of the International Association of Sedimentologists* **13**, 223–43.

McBride, E. F. 1974. Significance of color in red, green, purple, olive, brown, and gray beds of Difunta Group, northeastern Mexico. *Journal of Sedimentary Petrology* **44**, 760–73.

McBride, E. F., Weidie, A. E. & Wolleben, J. A. 1973. Deltaic and associated facies of Difunta Group (late Cretaceous to Paleocene), Parras and La Popa basins, Coahuila and Nuevo Leon, Mexico. *Transactions of Gulf Coast Association of Geological Societies* **23**, 37–40.

McPherson, J. G., Shanmugam, G. & Moiola, R. J. 1987. Fan-deltas and braid deltas: varieties of coarse-grained deltas. *Geological Society of America Bulletin* **99**, 331–40.

Melezhik, V. A. 1992. *Palaeoproterozoic sedimentary basins of the Baltic Shield*. St Petersburg: Nauka. [In Russian.]

Melezhik, V. A., Hudson-Edwards, K. A., Skuf'in, P. K. & Nilsson, L. P. 1994. Pechenga area, Russia – Part 1: Geological setting and comparison with Pasvik, Norway. *Transactions of the Institution of Mining and Metallurgy: Section B: Applied Earth Sciences* **103**, B129–45.

Melezhik, V. A., Sturt, B. A., Ramsay, D. M., Nilsson, L.-P. & Balashov, Yu. A. 1995. The early Proterozoic Pasvik-Pechenga Greenstone Belt: 1:200,000 geological map, stratigraphic correlation and revision in stratigraphic nomenclature. *Norges geologiske undersøkelse, Special Publication* **7,** 81–91.

Melezhik, V. A., Fallick, A. E. & Clark, T. 1997a. Two billion year old isotopically heavy carbon: evidence from the Labrador Trough, Canada. *Canadian Journal of Earth Sciences* **34**, 271–87.

Melezhik, V. A., Fallick, A. E. & Semikhatov, M. A. 1997b. Could stromatolite-forming cyanobacteria have influenced the global carbon cycle at 2300–2060 Ma? *Norges geologiske undersøkelse Bulletin* **433**, 30–1.

Melezhik, V. A., Fallick, A. E., Medvedev, P. V. & Makarikhin, V. V. 1999. Extreme $^{13}C_{carb}$ enrichment in ca. 2·0 Ga magnesite-stromatolite-dolomite-'red beds' association in a global context: a case for the world-wide signal enhanced by a local environment. *Earth-Science Reviews* **48**, 71–120.

Melezhik, V. A., Fallick, A. E., Medvedev, P. V. & Makarikhin, V. V. 2000. Palaeoproterozoic magnesite-stromatolite-dolomite-'red beds' association, Russian Karelia: palaeoenvironmental constraints on the 2·0 Ga positive carbon isotope shift. *Norsk Geologisk Tidsskrift* **80**, 163–86.

Melezhik, V. A., Fallick, A. E., Medvedev, P. V. & Makarikhin, V. 2001. Palaeoproterozoic magnesite: lithological and isotopic evidence for playa/sabkha environments. *Sedimentology* **48**, 379–97.

Melezhik, V. A., Fallick, A. E. & Grillo, S. M. 2004. Subaerial exposure surfaces in a Palaeoproterozoic ^{13}C-rich dolostone sequence from the Pechenga Greenstone Belt: palaeoenvironmental and isotopic implications for the 2330–2060 Ma global isotope excursion of $^{13}C/^{12}C$. *Precambrian Research* **133**, 75–103.

Melezhik, V. A., Fallick, A. E. & Kuznetsov, A. B. 2005. Palaeoproterozoic, rift-related, ^{13}C-rich, lacustrine carbonates, NW Russia. Part II: Global isotope signal recorded in the lacustrine dolostones. *Transactions of the Royal Society of Edinburgh: Earth Sciences* **95** (for 2004), 423–44.

Melezhik, V. A. & Fallick, A. E. 1996. A widespread positive $\delta^{13}C_{carb}$ anomaly at around 2·33–2·06 Ga on the Fennoscandian Shield: a paradox? *Terra Nova* **8**, 141–57.

Melezhik, V. A. & Fallick, A. E. 1997. Paradox regained? Reply. *Terra Nova* **9**, 148–51.

Melezhik, V. A. & Fallick, A. E. 2001. Proterozoic travertines of volcanic affiliation from a ^{13}C-rich rift lake environment. *Chemical Geology* **173**, 293–312.

Melezhik, V. A. & Sturt, B. A. 1994. General geology and evolutionary history of the early Proterozoic Polmak-Pasvik-Pechenga-Imandra/Varzuga-Ust'Ponoy Greenstone Belt in the northeastern Baltic Shield. *Earth-Science Reviews* **36**, 205–41.

Miall, A. D. 1977. A review of the braided-river depositional environment. *Earth-Science Reviews* **13**, 1–62.

Miall, A. D. 1984. Deltas. *In* Walker, R. G. (ed.) *Facies models*, 2nd edn. *Geoscience Canada, Reprint Series* **1**, 105–18.

Mints, M. V. 1993. Palaeotectonic reconstruction of the Early Precambrian in the Eastern Baltic Shield, Part 1: Early Proterozoic. *Geotectonica* **1**, 39–56. [In Russian.]

Muchane, M. W. 1996. Comparison of the isotope records in micrite, Lake Turkana, with the historical weather record over the last century. *In* Johnson, T. C. & Odada, E. O. (eds) *The limnology, climatology and paleoclimatology of the East African Lakes*, 431–41. Australia: Gordon & Breach.

Negrutza, V. S. 1984. *Early Proterozoic stages of evolution of the eastern part of the Baltic Shield*. Leningrad: 'Nedra'. [In Russian.]

Olsen, P. E., Kent, D. V., Cornet, B., Witte, W. K. & Schlische, R. W. 1996. High-resolution stratigraphy of the Newark rift basin (early Mesozoic, eastern North America). *Geological Society of America Bulletin* **108**, 40–77.

Petrov, V. P. & Voloshina, I. M. 1995. Regional metamorphism of the Pechenga area rocks. *In* Mitrofanov F. P. & Smol'kin, V. F. (eds) *Magmatism, sedimentogenesis and geodynamics of the Pechenga palaeorift*, 164–82. Apatity: Kola Science Centre. [In Russian.]

Picard, M. D. & High. L. R. 1981. Physical stratigraphy of ancient lacustrine deposits. *In* Ethridge, F. G. & Flores, R. M. (eds) *Recent and ancient nonmarine depositional environments: models for exploration. Society of Economic Paleontologists and Mineralogists Special Publication* **31**, 233–59.

Pokrovsky, B. G. & Melezhik, V. A. 1995. Variations of oxygen and carbon isotopes in Palaeoproterozoic carbonate rocks of the Kola Peninsula. *Stratigraphy and Geological Correlation* **3**, 42–53. [In Russian.]

Predovsky, A. A., Fedotov, Zh. A. & Akhmedov, A. M. 1974. *Geochemistry of the Pechenga complex*. Leningrad: Nauka. [In Russian.]

Predovsky, A. A., Melezhik, V. A., Bolotov, V. I., Fedotov, Zh. A., Basalaev, A. A., Kozlov, N. E., Ivanov, A. A., Zhangurov, A. A., Skuf'in, P. K. & Lubtsov, V. V. 1987. *Volcanism and sedimentology of the Precambrian in the north-eastern part of the Baltic Shield.* Leningrad: Nauka. [In Russian.]

Reading, H. G. & Collinson, J. D. 1996. Clastic coast. *In* Reading, H. G. (ed.) *Sedimentary environments: processes, facies and stratigraphy*, 3rd edn, 154–231. Oxford: Blackwell Science.

Reineck, H. E & Singh, I. B. 1980. *Depositional Sedimentary Environments*. Berlin: Springer-Verlag.

Renaut, R. W., Tiercelin, J. J. & Owen, R. B. 1986. Mineral precipitation and diagenesis in the sediments of the Lake Bogoria basin, Kenya Rift Valley. *In* Frostick, L. E., Renaut, R. W., Reid, I. & Tiercelin, J. J. (eds) *Sedimentation in the African Rifts. Geological Society Special Publication* **25**, 159–75.

Renaut, R. W., Jones, B. & Tiercelin, J. J. 1998. Rapid *in situ* silicification of microbes at Loburu hot springs, Lake Bogoria, Kenya Rift Valley. *Sedimentology* **45**, 1083–103.

Renaut, R. W., Morley, C. K. & Jones, B. 2002. Fossil hot-spring travertine in the Turkana Basin, northern Kenya: structure, facies, and genesis. *In* Renaut, R. W. & Asley, G. M. (eds) *Sedimentation in continental rifts. Special Publication of the Society of Economic Paleontologists and Mineralogists* **73**, 123–41.

Renaut, R. W. & Jones, B. 1997. Controls on aragonite and calcite precipitation in hot spring travertines at Chemurkeu, Lake Bogoria, Kenya. *Canadian Journal of Earth Sciences* **34**, 801–18.

Renaut, R. W. & Owen, R. B. 1998. Opaline cherts associated with sublacustrine hydrothermal springs at Lake Bogoria, Kenya Rift Valley. *Geology* **16**, 699–702.

Renaut, R. W. & Tiercelin, J. J. 1994. Lake Bogoria, Kenya Rift valley – a sedimentological overview. *In* Renaut, R. W. & Last, W. M. (eds) *Sedimentology and geochemistry of modern and ancient saline lakes. Society of Economic Paleontologists and Mineralogists Special Publication* **50**, 101–23.

Schidlowski, M., Eichmann, R. & Junge, C. E. 1976. Carbon isotope geochemistry of the Precambrian Lomagundi carbonate province, Rhodesia. *Geochimica et Cosmochimica Acta* **40**, 449–55.

Schottle, M. & Müller, G. 1968. Recent carbonate sedimentation in the Gnadensee (Lake Constance), Germany. *In* Müller, G. & Friedman, G. M. (eds) *Recent developments in carbonate sedimentology in Central Europe*, 148–56. Berlin: Springer-Verlag.

Sharkov, E. & Smolkin, V. F. 1997. The early Proterozoic Pechenga-Varzuga Belt: a case of back-arc spreading. *Precambrian Research* **82**, 135–51.

Shinn, E. A. 1983: Tidal flat environment. *In* Scholle, P. A., Bebout, D. G. & Moore, C. H. (eds): *Carbonate depositional environments*, 173–210. *Memoir* **33**. Tulsa, OK: American Association of Petroleum Geologists.

Skuf'in, P. K. 1993. Evolution of volcanism of the metalliferous Pechenga zone. *Geology of Ore Deposits* **35**, 271–83. [In Russian.]

Smoot, J. P. 1991. Sedimentary facies and depositional environments of early Mesozoic Newark Supergroup basins, eastern North America. *Palaeogeography, Palaeoclimatology, Palaeoecology* **84**, 369–423.

Smoot, J. P. & Lowenstein, T. K. 1991. Depositional environments of non-marine evaporites. *In* Melvin, J. L. (ed.) *Developments in sedimentology* **50**, 189–347. Amsterdam: Elsevier.

Sochava, A. V. 1979. *Precambrian and Phanerozoic 'red beds'*. Leningrad: Nauka [In Russian.]

Southgate, P. N. 1986. Depositional environment and mechanism of preservation of microfossils, upper Proterozoic Bitter Springs Formation, Australia. *Geology* **14**, 683–6.

Sreenivas, B., Kumar, B., Srinivasan, R. & Roy, A. B. 1996. Carbon and oxygen isotope composition of the carbonate rocks of the Proterozoic Aravalli Supergroup, Udaipur region, Rajasthan, India: evidence for heavy δ^{13}C excursion. *In* Aggarwal, S. K. & Jain, H. C. (eds) *Seventh National Symposium on Mass Spectrometry*, DRDE, Gwalior, 26–28 November, 1996, 428–31.

Srivastava, N. K. & Almeida L. B. de. 2000. *Lagoa Salgada (Rio de Janeiro): recent stromatolites*. During-congress field trip. 31st International Geological Congress, Rio de Janeiro, Brazil, 6–17 August, 2000. Field trip DFT 12.

Strong, A. E. & Eadie, B. J. 1978. Satellite observations of calcium carbonate precipitations in the Great Lakes. *Limnology and Oceanography* **23**, 877–87.

Sturt, B. A., Melezhik, V. A. & Ramsay, D. M. 1994. Early Proterozoic regolith at Pasvik, NE Norway: palaeoenvironmental implications for the Baltic Shield. *Terra Nova* **6**, 618–33.

Szulc, J., Roger, Ph., Mouline, M. P. & Lenguin, M. 1991. Evolution of lacustrine systems in the Tertiary Narbonne Basin, northern Pyrennean foreland, southeast France. *In* Anadón, P., Cabrera, L. I. & Kelts, K. (eds) *Lacustrine facies analysis. Special Publication of International Association of Sedimentologists* **13**, 279–90.

Talbot, M. R. & Allen, P. A. 1996. Lakes. *In* Reading, H. G. (ed.) *Sedimentary environments: processes, facies and stratigraphy*, 3rd edn., 83–124. Oxford: Blackwell.

Tucker, M. E. 1978. Triassic lacustrine sediments from South Wales: shore-zone clastics, evaporites and carbonates. *In* Matter, A. & Tucker, M. E. (eds) *Modern and ancient lake sediments. Special Publication of International Association of Sedimentologists* **2**, 205–24.

von der Borch, C. C. 1976. Stratigraphy of stromatolite occurrences in carbonate lakes of the Coorong Lagoon area, South Australia. *In* Walter, M. R. (ed.) *Stromatolites*, 413–20. Amsterdam: Elsevier.

Zagorodny, V. G., Mirskaya, D. D. & Suslova, S. N. 1964. *Geology of the Pechenga sedimentary-volcanogenic series*. Leningrad: Nauka. [In Russian.]

V. A. MELEZHIK, Geological Survey of Norway, Leiv Erikssons vei 39, N-4791, Trondheim, Norway.

A. E. FALLICK, Scottish Universities Environmental Research Centre, East Kilbride, Glasgow G75 0QF, Scotland.
e-mail: T.Fallick@suerc.gla.ac.uk

MS received 22 April 2003. Accepted for publication 12 May 2004.